BULLETIN OF THE EARTHQUAKE
RESEARCH INSTITUTE
UNIVERSITY OF TOKYO
Vol. 67 (1992) pp. 479–512

Report on DELP 1989 Cruise in the TTT Junction Areas Part 2: Upper Crustal Structure Near the Trench-Trench-Trench Triple Junction off the Boso Peninsula, Japan

Naoshi HIRATA[1*****], Narumi TAKAHASHI[1], TOSHIYUKI AMISHIKI[1*], Hiroshi KATAO[2**], Yuka KAIHO[3***], Shizuo KASHIWABARA[4], Ryota HINO[5], Hisatoshi BABA[6], Hajime SHIOBARA[7], Sadayuki KORESAWA[2], Masanao SHINOHARA[1****], Atsuki KUBO[8], Toshihiko KANAZAWA[3], Junzo KASAHARA[2] and Hajimu KINOSHITA[1*****]

[1)]Department of Earth Sciences, Chiba University, Chiba 263
[2)]Earthquake Research Institute, the University of Tokyo, Tokyo 113
[3)]Faculty of Science, the University of Tokyo, Tokyo 113
[4)]Japan Meteorological Agency, Tokyo 100
[5)]Observation Center for Prediction of Earthquake and Volcanic Eruptions, Faculty of Science, Tohoku University, Sendai 980
[6)]School of Marine Science and Technology, Tokai University, Shimizu 424
[7)] Laboratory for Ocean Bottom Seismology, Hokkaido University, Sapporo 060
[8)] Department of Earth Sciences, Kobe University, Kobe 657

(Received September 29, 1992)

Abstract

In July 1989 twenty-two ocean bottom seismographs (OBSs) from 5 Japanese institutions were deployed in an array on the deep sea floor in the vicinity of the trench-trench-trench triple junction off the Boso Peninsula, Japan. The array is 300 km long and 80 km wide, including 3 profiles for study of crustal structure. A permanent OBS array telemetered by a cable system (Japan Meteorological Agency) was used as a part of the array. The sea floor array was complemented by five temporary land stations on the Boso Peninsula. Water depth along the seismic profile varies considerably from a few 100 m to 9000 m or more. We placed three OBSs specially designed for the very deep ocean.

We conducted airgun-OBS profiling for the refraction survey. Two 16-liter airguns were fired every 40–50 s spaced about 100 m apart. Airgun signals were observed as far as 30–40 km from the OBS. To obtain the sedimentary and shallow crustal structure we transformed seismograms of airgun shots into the intercept time (τ)-ray parameter (p) domain and inverted them in a P-wave speed structure with depth by the τ-sum inversion method.

*Present address: Furukawa commercial high school, Furukawa 989-61, Japan
**Present address: Abuyama Observatory, Kyoto University, Osaka 569, Japan
***Present address: Japan Marine Science and Technology Center, Yokosuka 237, Japan
****Present address: Ocean Research Institute, the University of Tokyo, Tokyo 164, Japan
*****Present address: Earthquake Research Institute, the University of Tokyo, Tokyo 113, Japan

We derived one-dimensional models for all OBSs. Both the sedimentary thickness and the P-wave speed in the sedimentary layer change along the profiles. The difference in sedimentary structure between the oceanic side of the trench axis and the continental side is evident: the sediment on the pacific plate consists of a vertically homogeneous unconsolidated layer (0.32 s^{-1} of vertical wave speed gradient) and a consolidated layer with a large gradient of 4.8 s^{-1}, while on the Northeast Japan plate the gradient is 0.65 s^{-1} in the topmost and 0.8 s^{-1} in the lower part of the sediment.

1. Introduction

The triple junction off central Japan, which is named the Off-Boso triple junction by the Hydrographic Department of the Maritime Safety Agency of Japan, is located at the intersection of the Japan, Izu-Bonin, and Sagami Trenches: The Japan Trench is the boundary between the Pacific and the Northeast Japan plates. The Izu-Bonin Trench runs between the Pacific and the Philippine Sea plates, and the Sagami Trough runs between the Philippine Sea and the Northeast Japan plates.

The junction is the only known example of the TTT(a)-type triple junction defined by MCKENZIE and MORGAN (1969). The triple junction is unstable because the Philippine Sea plate currently moves west-northwest with respect to northeast Japan: the direction is subparallel to the trend of the Sagami Trough. If the plates are completely rigid, geometrical consideration of plate tectonics leads to westward migration of the Izu-Bonin Trench with respect to the Pacific plate. Or, if the Izu-Bonin Trench retains its position with respect to other plates, there must be internal deformation within the plates. The very deep water depth of more than 9000 m in the vicinity of the triple junction can be attributed to crustal deformation due to the unstable geometry of the three plates.

To understand the structure, dynamics, and evolution of the triple junction, many geophysical and geological investigations, including seismic, magnetic, and gravity surveys, were carried out. Until recently, however, details of the morphology and the structure near the junction were poorly known because of the large depth of water: No deep seismic refraction study in the vicinity of the junction was conducted. Among recent surveys with SeaBeam are those during the French-Japanese Kaiko project in 1984 (KINOSHITA *et al.*, 1986; RENARD *et al.*, 1987; OGAWA *et al.*, 1989; SENO *et al.*, 1989) and those by the Hydrographic Department of the Maritime Safety Agency of Japan (KATO *et al.*, 1985). Multichannel seismic reflection surveys were also conducted in the junction area (TAIRA *et al.*, 1988; IWABUCHI *et al.*, 1990).

Recent development of ocean bottom seismology enables us to obtain a detailed image of the crustal structure in the deep ocean. In the western Pacific margin of the subduction zone are several deep seismic sounding surveys: the Kuril, the Japan, and the Ryukyu Trench areas were investigated by ocean bottom seismographic (OBS) arrays using controlled seismic sources (IWASAKI *et al.*, 1989, 1990).

In July 1989 the triple junction off central Japan was covered by an array of OBSs for the first time to study the crustal and the upper mantle structure of the junction off the Boso Peninsula. Twenty-two OBSs from five Japanese institutions were deployed in an array on the deep sea floor. The array is 300 km long and 80 km wide, including 3 profiles

for study of the crustal structure. An airgun array and explosives were used as controlled seismic sources. We will report here on the experiment and the preliminary results on the seismic structure. We will focus on the airgun-OBS profiling survey. The data and results from the refraction survey using explosives are presented elsewhere.

2. Experiments

2.1. Airgun profiling

We shot four airgun profiles denoted as Lines 1, 2, 4, and 5 in Fig. 1: Line 1 is 110 km long running toward N25°E. The profile covers the northern tip of the Philippine Sea plate and northeastern Japan, which is thought to be part of the North American plate. Line 2 runs 90 km toward N60°E. The main E-W profile running toward E20°S consists of Lines 4 and 5: Line 4 is 140 km long and Line 5 is 110 km long (Fig. 1). An array of airguns, which consisted of two 16-liter BOLT type airguns, was fired at intervals of 40 s or 50 s. The ship ran at a speed of about 5 kt (9 km/h) to give shots every 100 or 125 m. Signals from the airgun array were recorded by a single channel seismic profiling (SCS) system and, simultaneously, by an array of ocean bottom seismographs (OBSs): the SCS provided reflection data and the OBSs gave us refraction data.

2.2. Ocean bottom seismographic array

Five types of OBSs were used, which were developed in four institutions of three universities. One type is newly developed for very deep ocean bottom greater than 7000

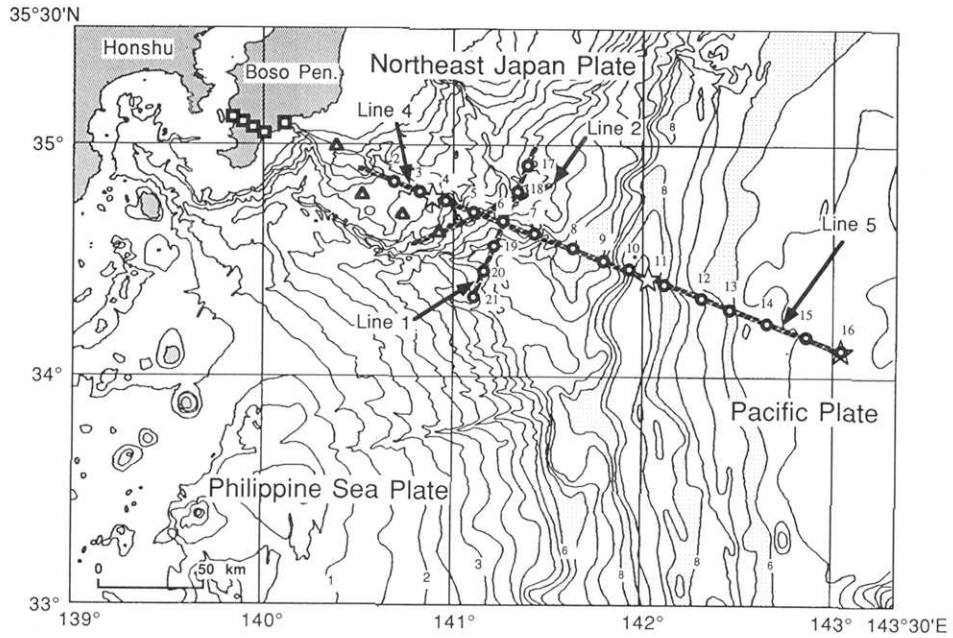

Fig. 1. Location of ocean bottom seismographic (OBS) array and lines of airgun-OBS profiling. Open circles, triangles, and squares show temporary OBSs, OBSs of JMA, and temporary land stations, respectively. Airgun profiling lines are denoted by shaded lines. Asterisks are positions of large explosions.

m (KANAZAWA and KAIHO, 1990). Details of individuals OBSs are seen in YAMADA *et al.* (1981), NAGUMO *et al.* (1982), MATSUDA *et al.* (1986), and BABA *et al.* (1988). In general, however, characteristics of the instruments are almost the same: each OBS is equipped with a vertical and one or two horizontal geophones with natural frequencies ranging from 2 to 4.5 Hz. Some OBSs have a hydrophone, which is useful to detect signals propagated through water. Seismic signals were recorded by the direct analog recording (DAR) method. The signals recorded by the DAR method cover frequency range between a few hertz and 30 Hz. Details of the position and components of observed signals are tabulated in Table 1. Retrieval of the OBS is completed by transmitting acoustic signals from the ship to command the OBS to release an anchor. Two OBSs have a preprogrammed timer to release the anchor.

We relocated OBS positions according to travel times of water waves. First we fixed the position at which the airgun was shot using the LORAN-C navigation data. Since the LORAN-C data are often scattered up to several hundred meters, we smoothed the position data, which were recorded every four seconds, by averaging them. And we estimated the position at which the airgun was shot. Then we estimated the location of bottoming of an OBS from travel times of the direct water waves observed by the OBS with respect to fixed shot positions. We used the travel times of the water waves from the airgun shooting within an offset range of 15 km. OBSs near two profiling lines are well located because the shot positions are distributed two-dimensionally. However,

Table 1. OBS location of the 1989 DELP Triple Junction experiment

OBS	Institution	Recording Period		Location		Remarks	Line
		Deployment (JST)	Retrieval (JST)	Latitude N	Longitude E	Depth (m)	
TJ2	GIT	Jul. 10 20:49	Jul. 21 12:02	34° 50.99'	140° 40.13'	1795.1 Good	4
TJ3	ERI	Jul. 10 22:00	not retrieved	34° 48.58' *	140° 48.12' *	2026.0 ------	4
TJ4	GIT	Jul. 10 23:00	Jul. 21 6:50	34° 46.16'	140° 56.48'	2935.5 Good	4
TJ5	CHU	Jul. 11 0:23	Jul. 21 4:22	34° 42.97'	141° 7.44'	4291.5 Good	2,4
TJ6	ERI	Jul. 11 1:34	Jul. 21 1:20	34° 38.89'	141° 17.32'	4919.0 Good	1,4
TJ7	GIT	Jul. 11 2:45	Jul. 20 21:42	34° 36.35'	141° 28.31'	5583.3 Good	4
TJ8	ERI	Jul. 11 3:41	Jul. 20 18:18	34° 34.04'	141° 36.26'	5450.0 Good	4
TJ9	CHU	Jul. 11 4:41	not retrieved	34° 31.35' *	141° 45.14' *	6364.0 ------	4
TJ10	GIT	Jul. 15 3:27	Jul. 20 10:16	34° 29.07'	141° 53.82'	7904.6 Cross talk	5
TJ11	GIT	Jul. 15 4:25	Jul. 19 16:38	34° 25.40'	142° 8.35'	7977.3 Cross talk	5
TJ12	GIT	Jul. 15 5:08	not retrieved	34° 20.98' *	142° 18.92' *	7142.0 ------	5
TJ13	ERI	Jul. 14 0:24	Jul. 19 21:35	34° 18.73'	142° 27.26'	6000.0 Good	5
TJ14A	TKS	Jul. 14 2:25	Jul. 19 5:19	34° 15.48'	142° 38.31'	5725.6 Poor	5
TJ14B	LOBS	Jul. 14 2:26	Jul. 19 5:14	34° 15.15'	142° 38.17'	5558.7 Good	5
TJ15	CHU	Jul. 14 3:56	Jul. 19 1:25	34° 11.13'	142° 52.13'	5275.9 Noisy	5
TJ16	ERI	Jul. 14 5:34	Jul. 18 22:13	34° 6.91'	143° 4.02'	5260.0 Good	5
TJ17	ERI	Jul. 11 7:55	Jul. 21 17:53	34° 55.07'	141° 24.73'	3950.0 Good	1
TJ18	CHU	Jul. 11 9:08	Jul. 21 18:42	34° 49.39'	141° 22.05'	3536.3 Good	1,2
TJ19	GIT	Jul. 11 11:37	Jul. 21 23:09	34° 34.73'	141° 13.44'	6361.7 Good	1
TJ20	TKS	Jul. 11 13:05	Jul. 22 1:17	34° 25.10'	141° 9.82'	6377.3 Good	1
TJ21A	CHU	Jul. 11 14:33	Jul. 22 4:36	34° 13.33'	141° 5.12'	5270.4 Good	1
TJ21B	LOBS	Jul. 11 14:35	Jul. 22 5:08	34° 14.99'	141° 5.02'	5297.9 Good	1
BOSO1	JMA			34° 42.53'	140° 58.55'	4074.0 Good	2
BOSO2	JMA			34° 45.08' *	140° 45.27' *	2090.0 Poor	4
BOSO3	JMA			34° 48.10' *	140° 30.62' *	1898.0 Poor	4
BOSO4	JMA			34° 59.40' *	140° 20.28' *	658.0 Poor	4

ERI: Earthquake Research Inst., Univ. of Tokyo, GIT: Geophysical Inst., Univ. of Tokyo, CHU: Chiba Univ. TKS: Tokai Univ., LOBS: Laboratory for Ocean Bottom Seismology, Hokkaido Univ., JMA: Japan Meteorological Agency

*Ship position at which the OBS was deployed. Without an asterisk, the OBS location was relocated due to travel times of water waves.

locations of OBSs on a single profiling line are under-determined by only the travel time data. So we incorporated prior information on the location from a Bayesian point of view (JACKSON and MATSU'URA, 1985); we used the midpoint between the launching and the recovery of the OBS as the prior location of the OBS position with its uncertainty (one standard error) of half of the difference between them. We located the OBS using those prior data and observed travel time data by the same algorithm as used in hypocenter location of HIRATA and MATSU'URA (1987).

We show an example of comparison in Fig. 2, where the ship position at which an OBS was deployed, the relocated OBS position, and the ship position at which the OBS was retrieved are displayed. The OBS (TJ5) was moved northeast during operations of deployment and retrieval of the OBS due to a strong sea water current. Usually the difference between the deployed and retrieved position is about 0.5–1.0 n.m. (1–2 km). The relocated position, at which the OBS was located on the sea bottom, was usually approximately between the deployed and the retrieved positions.

A permanent OBS array telemetered by a cable system of the Japan Meteorological Agency (FUJISAWA *et al.*, 1986) was used as part of the array, the position of which is shown in Fig. 1.

2.3. Temporary land station on the Boso Peninsula

The sea floor seismographic array was complemented by four temporary land stations on the Boso Peninsula, and one permanent station at the Kominato Marine Laboratory, Marine Ecosystems Research Center, Chiba University (HIRATA *et al.*, 1990). The temporary stations were installed for six days. Each station was equipped with one vertical and one horizontal 4.5-Hz geophones, outputs of which were recorded

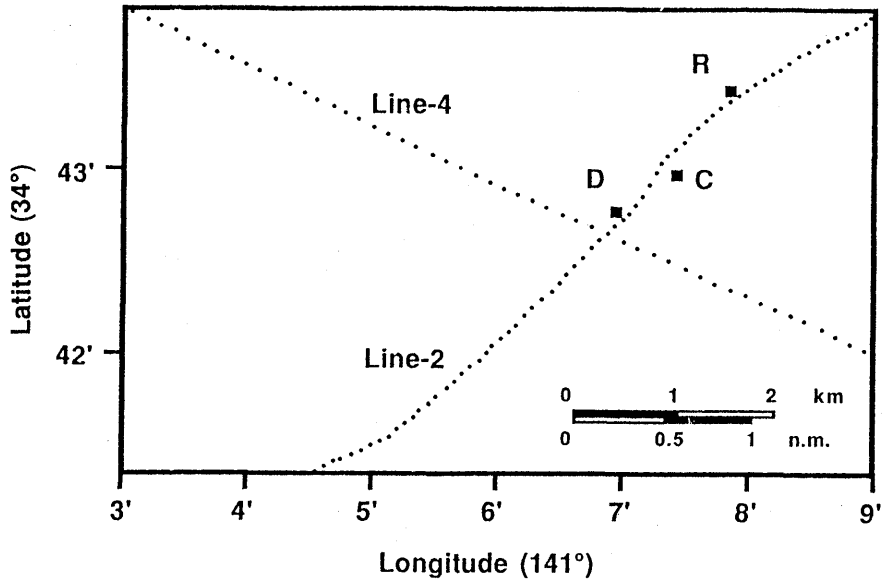

Fig. 2. Example of comparison among locations of TJ5 during operation. Deployed position (D), relocated position at sea bottom (C), and retrieved position (R) are shown, indicating drifting of the OBS during bottoming and floating due to a strong water current toward the northeast. Small dots are positions at which airguns were shot.

Table 2. Temporary land stations

Station code	Location			Period
	Latitude N	Longitude E	Height (m)	
ST1	35° 03'44.3"	140° 00'01.8"	70	Jul.15-Jul.20
ST2	35° 04'18.4"	139° 57'51.0"	95	Jul.15-Jul.20
ST3	35° 05'36.0"	139° 54'28.8"	105	Jul.15-Jul.20
ST4	35° 06'19.3"	139° 52'12.0"	115	Jul.15-Jul.20
KMT	35° 03'03.9"	140° 11'15.4"	10	Jul.

KMT: Kominato Marine Laboratory, Marine Ecosystems Research Center, Chiba University

by the DAR method as was used in the OBSs. Details of the locations and the recording periods are summarized in Table 2.

3. Single channel seismic profiling (SCS)

3.1. Data acquisition

We acquired signals from the airgun shooting both by a single channel hydrophone streamer (SCS) and by the OBS array. The SCS data were recorded on board in analog and digital forms. The analog records were displayed on a chart recorder. The digital records were stored in a hard disk unit through a personal computer (SHINOHARA *et al.*, 1989).

The digital acquisition system was newly developed and tested in the experiment. It included a recording amplifier with analog filters (8–125 Hz), a 12 bit-resolution analog-to-digital converter, and a 40 MB hard disk. We stored the data of every other shot on Line 1 for 20 s at a sampling rate of 200 Hz. On Lines 2, 4, and 5, signals of every shot were recorded for 16 s at a rate of 500 Hz.

The digitally recorded reflection data were processed on shore. We performed band pass filtering and deconvolution of reverberations due to bubble oscillation of the airgun signal. The pass frequency band was from 20 to 50 Hz. For display, each trace was equalized such that the sum of squares of amplitudes for one second was constant for the entire trace: We show processed reflection profiles in Figs. 3, 4, 5, and 6 with our interpretations of the records.

3.2. Seismic stratigraphy

Reflection data of Line 1 show two acoustic units: We call them Bonin 1 and Bonin 2 hereafter (Fig. 3). Bonin 1, the upper layer, is acoustically transparent and shows clear stratified reflectors in the unit. It has the maximum thickness of 1.0 s of two way travel time (TWT). Between Bonin 1 and Bonin 2 is an evident reflector forming an acoustic basement. Bonin 2 is acoustically opaque and no clear reflector is recognized in it. We can trace Bonin 1 up to the brink of the Boso Canyon and Bonin 2 up to the center of the canyon. Within the range between 45 km and 65 km in Fig. 3 is a steep landward slope of the Sagami Trough. The water depth changes by 3.3 km over a horizontal distance of 30 km. There are several steep steps which we can commonly observe in the landward slope of other trenches (e.g., in the Japan Trench, LUDWIG. *et al.*, 1966). Beneath the slope

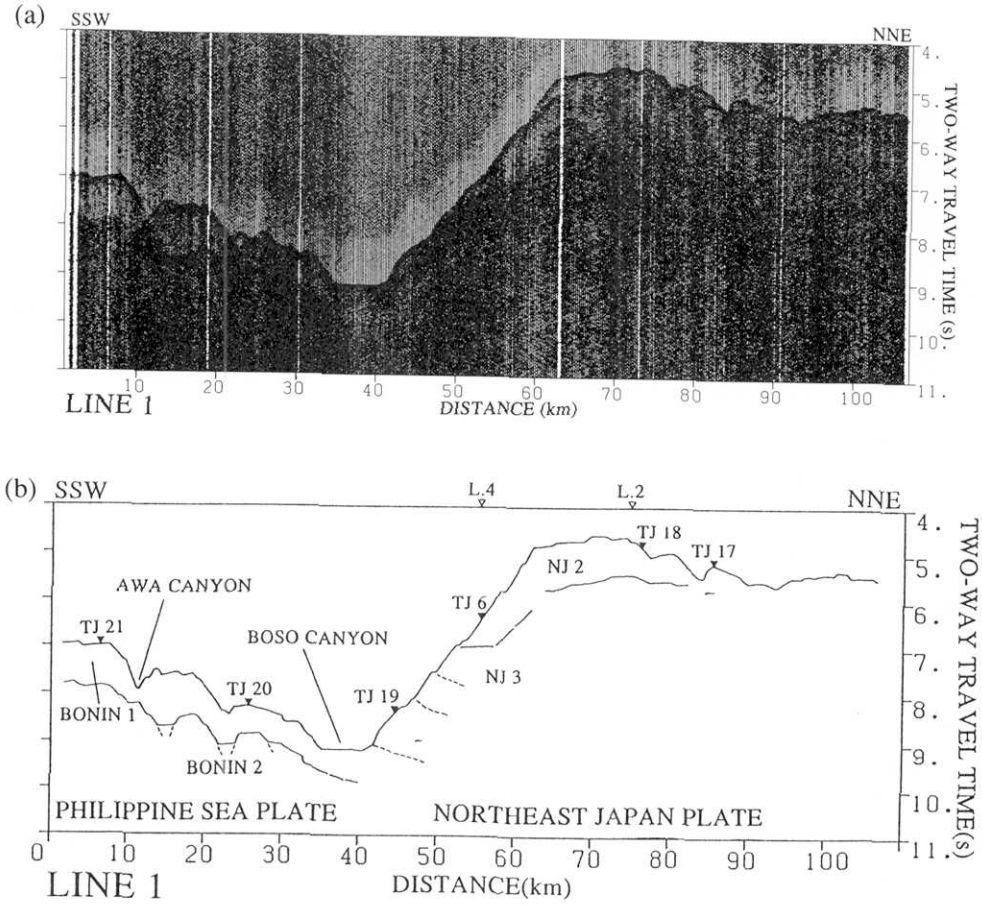

Fig. 3. Single channel seismic (SCS) profile of Line 1. (a) Time section of records. Band pass (20–50 Hz) and deconvolution (0.2 s) filters are applied. The trace amplitude is equalized. See text for details. Horizontal distance is measured from the southern end of Line 1 (34° 12' 12.3''N, 141° 2' 51.3''). (b) Interpretation of (a). Solid triangles denote positions of OBSs. Open triangles show intersections with Lines 2 and 4.

is a change in acoustic characteristics of reflection at 7.0 s TWT. We divided the layer into two acoustic units: the unit above the 7.0 s TWT is referred to as NJ 2, and the unit below it is NJ 3. No clear reflector is found beneath the slope.

Line 2 covers the Katakai Canyon and the Katsu'ura Canyon. We can see two acoustic units in the profile (Fig. 4). The upper unit, which corresponds to NJ 2 on Line 1, varies in thickness having its maximum at 1.5 s TWT. The upper unit disappears near the southwestern end of the profile and the lower unit, NJ 3, is exposed on sea floor there. The signal-to-noise ratio of the profile is not sufficient to identify the an internal structures of these units.

The E-W main profile consists of Lines 4 and 5. Line 4 covers the continental slope including the Katsu'ura Canyon and the Katakai Canyon. We can see three acoustic units (Fig. 5): The uppermost unit, which is referred to as NJ 1 hereafter, appears at the sea floor in the range of 0–55 km. The middle unit, NJ 2, forms the sea bottom in the range of 55–90 km. The lowermost unit, NJ 3, can be seen as the sea bottom in the range of 90–100

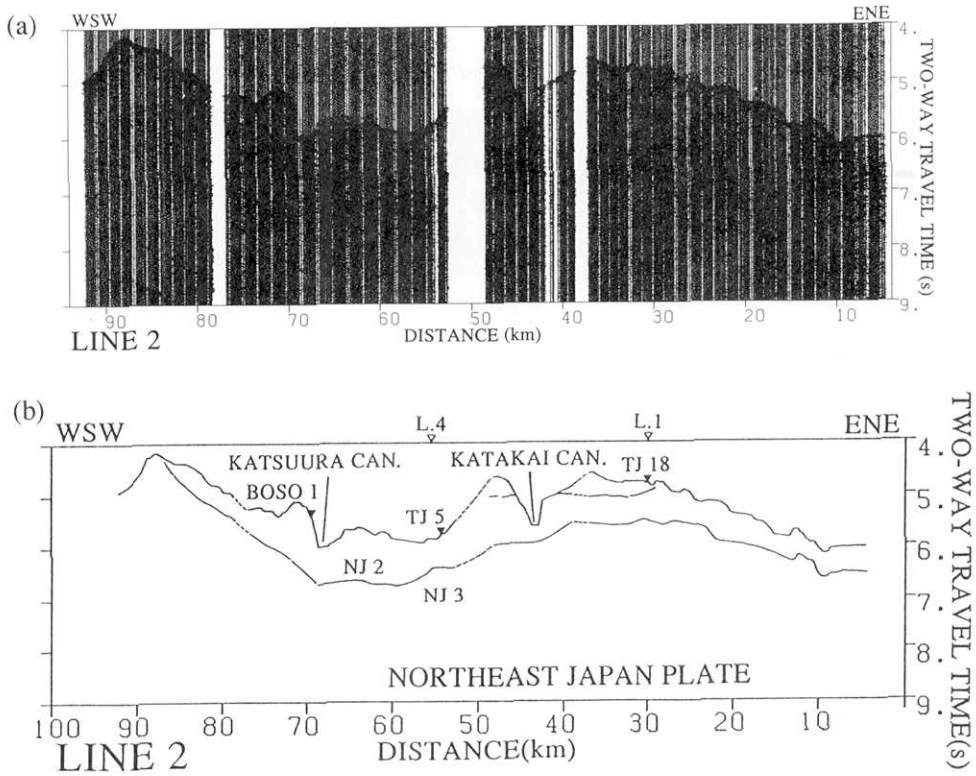

Fig. 4. SCS profile of Line 2. Parameters for plotting are the same as in Fig. 3 except for the origin of the distance (35° 2' 19.0"N, 141° 34' 32.8"E). (a) Time section of records. (b) Interpretation of (a). Open triangles show intersections with Lines 1 and 4.

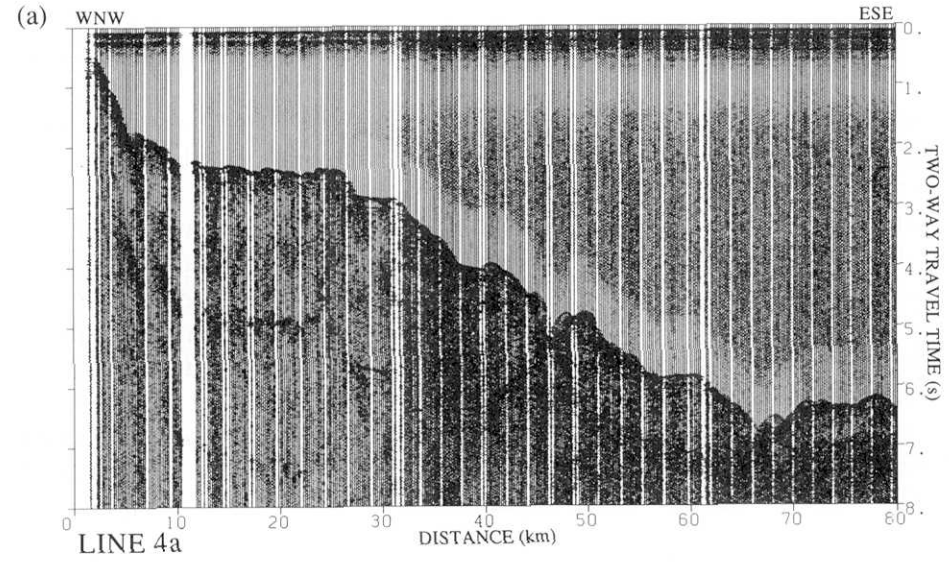

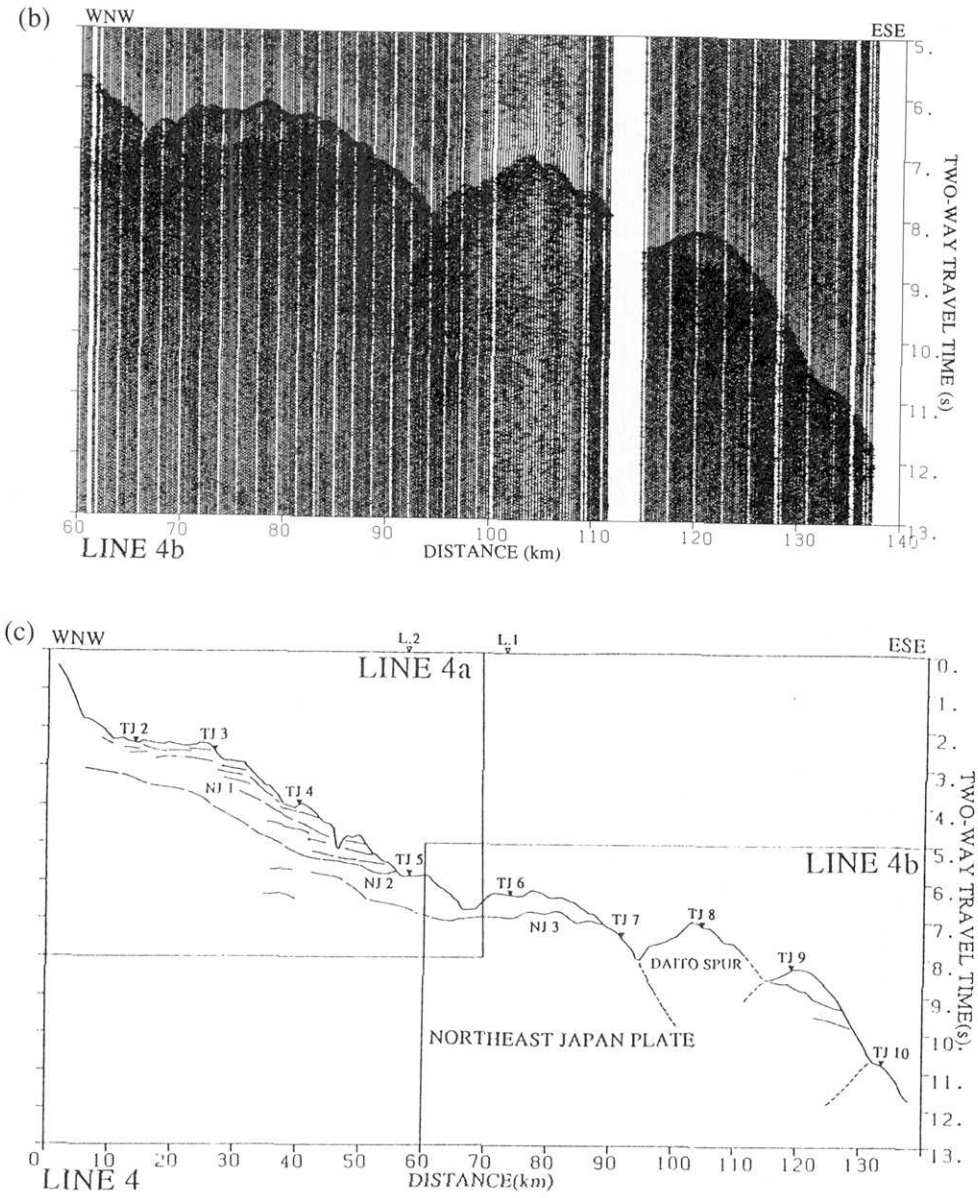

Fig. 5. SCS profile of Line 4. Parameters for plotting are the same as in Fig. 3 except for the origin of the distance (35° 53' 28.4"N, 141° 31' 30.9"E). (a) Time section of records within distances between 0 and 80 km. (b) Time section of records within distances between 60 and 140 km. (c) Interpretation of the record section. Rectangles show the areas shown in (a) and (b). Open triangles show intersections with Lines 1 and 2.

km. The uppermost unit, NJ 1, is the most transparent among the three units, and has some clear reflectors.

Line 5 spans from the trench axis to the Pacific Basin (Fig. 6). The trench axis is filled with a thick sediment of 2.0 s TWT including many stratified reflectors. Beyond 65 km is a clear transparent unit, which is referred to as Pac 1. Pac 1 has a thickness from 0.4

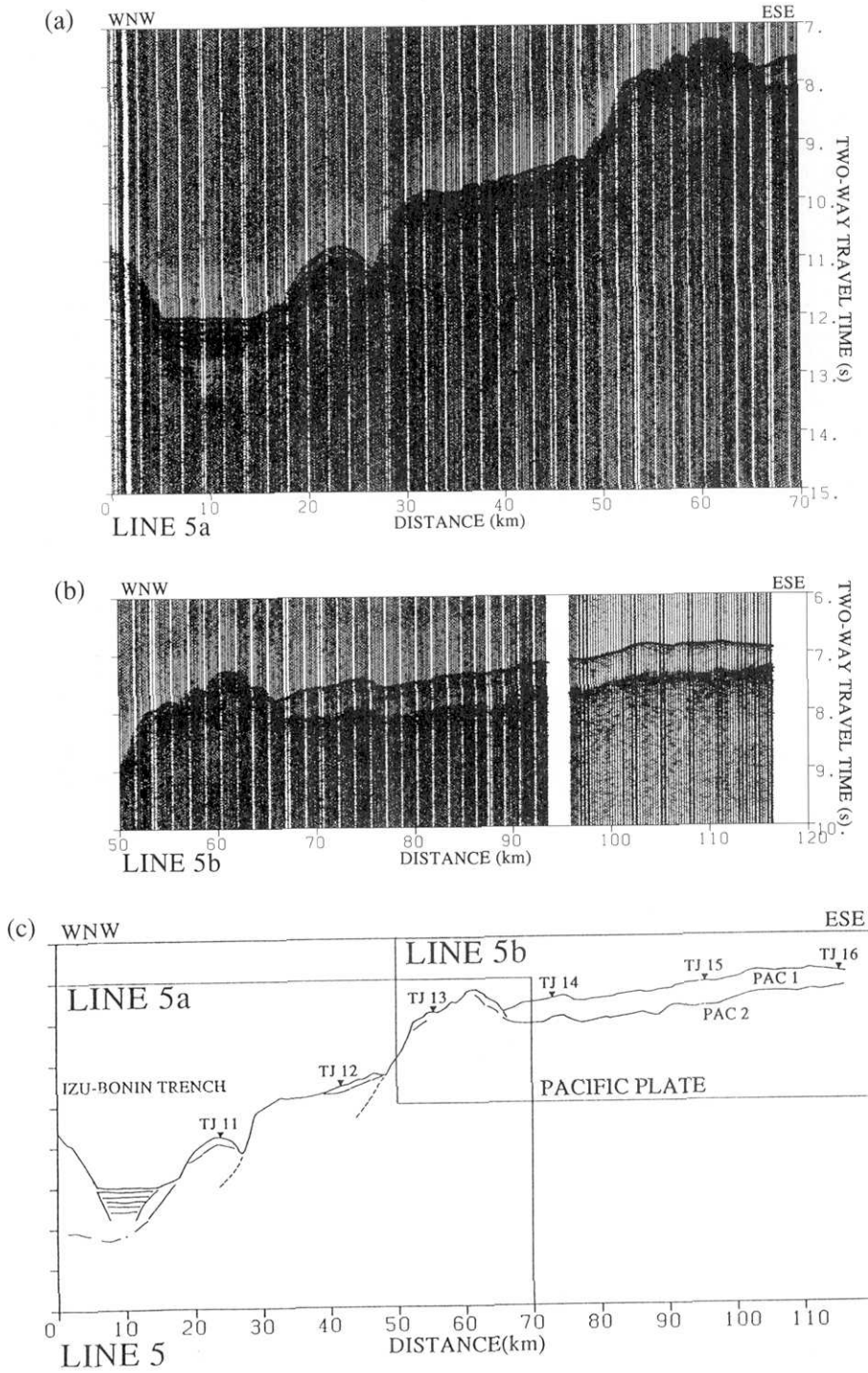

Fig. 6. SCS profile of Line 5. Parameters for plotting is the same as in Fig. 3 but for the origin of the distance (34° 29' 2.0"N, 141° 53' 18.2"E). (a) Time section of records within distances between 0 and 70 km. (b) Time section of records within distances between 50 and 120 km. (c) Interpretation of the record section. Rectangles show the areas shown in (a) and (b).

to 0.7 s TWT. Below Pac 1 is an acoustic basement, which is referred to as Pac 2. Between 20 and 65 km are some areas with thin sediment, but most parts are occupied by an acoustically opaque material, which is divided by near vertical displacements.

4. OBS-airgun profiling

4.1. OBS recorded airgun data

All OBS records were converted in a digital form with a sampling rate of approximately 100 samples per second after the cruise. We followed URABE and HIRATA (1984). The digitized data were edited and processed for further analysis. The data were exchanged among different institutions.

We show processed OBS records on four lines. Figure 7 displays record sections of a vertical component on Line 1. Records from Line 2 are in Fig. 8, those from Line 4 are in Fig. 9, and those from Line 5 are in Fig. 10. The data were filtered with a pass band between 5 and 15 Hz. In general, we can recognized refracted wave up to an offset distance of 45 km. An example of the OBSs located on the Philippine Sea plate is TJ21, the record section of which is shown in Fig. 7f. In the offset range between 8 and 40 km we can see a phase with an apparent speed of 5 km/s. A 2.5 km/s phase is seen in a low gain channel of the record later than the water wave arrivals. Travel time curves of these phases are almost straight lines, indicating a small gradient with depth.

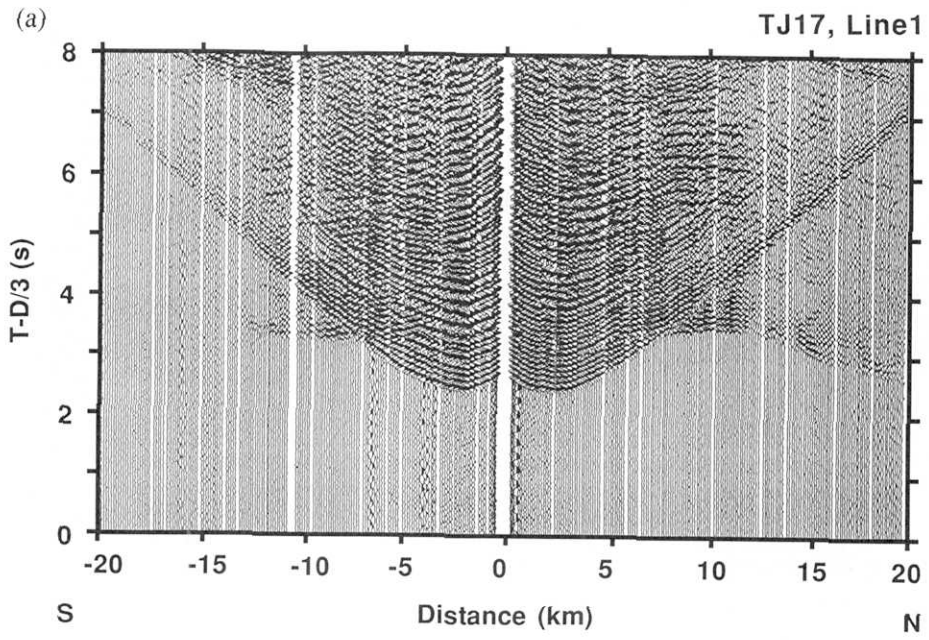

Fig. 7. Airgun signal recorded by OBSs on Line 1. Vertical component of the geophone with high gain amplification is shown. Travel times are reduced by D/(3.0 km/s), where D is an offset distance from the OBS in km. the horizontal axis is D in km. The records are bandpass filtered (5 to 15 Hz). Each trace except that of TJ21B is scaled proportional to D square. Traces of TJ21B are normalized by the maximum amplitude. (a) TJ19. (b) TJ18. (c) TJ6. (d) TJ19. (e) TJ20. (f) TJ21A. (g) TJ21B.

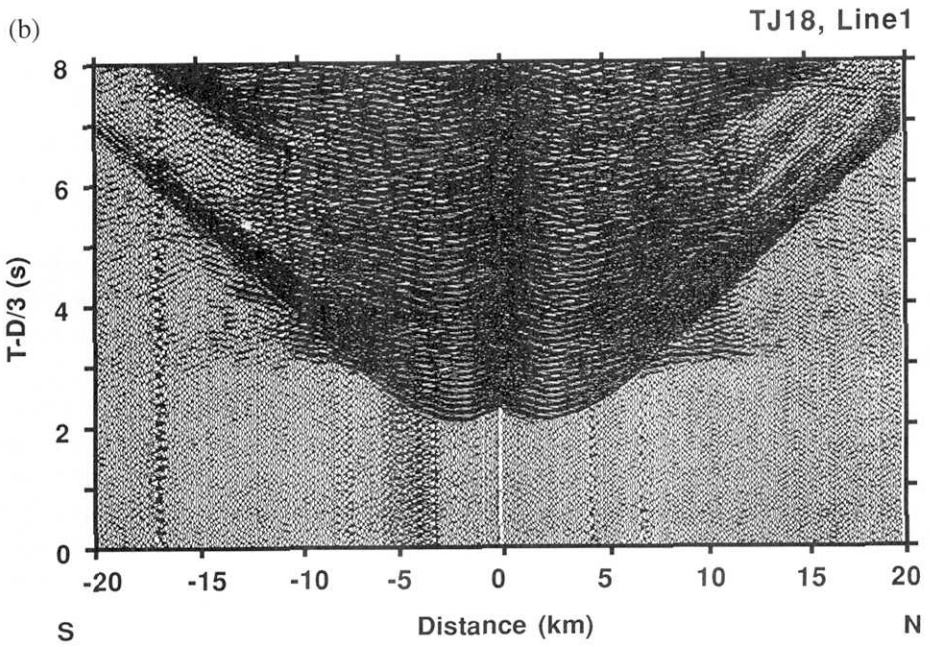
(b)
TJ18, Line1
T-D/3 (s)
8
6
4
2
0
-20
-15
-10
-5
0
5
10
15
20
S
Distance (km)
N

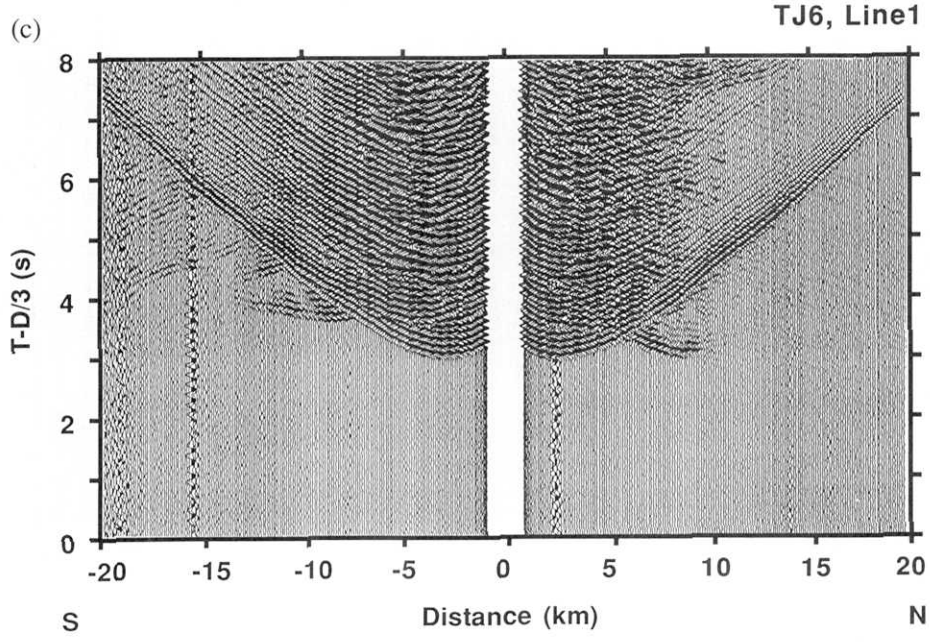
(c)
TJ6, Line1
T-D/3 (s)
8
6
4
2
0
-20
-15
-10
-5
0
5
10
15
20
S
Distance (km)
N

(d)

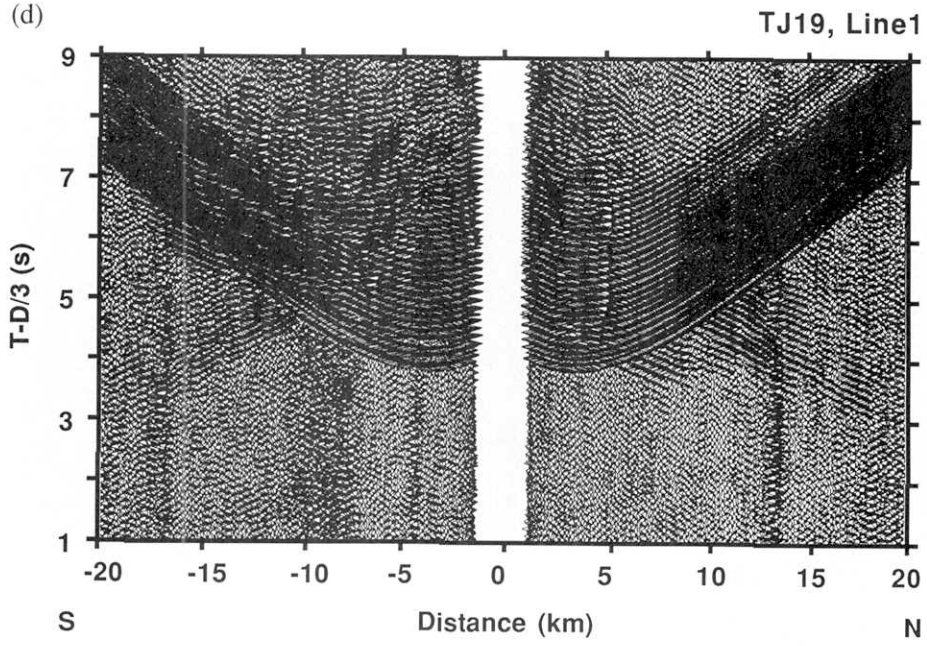
TJ19, Line1
T-D/3 (s)
9
7
5
3
1
-20
-15
-10
-5
0
5
10
15
20
S
Distance (km)
N

(e)

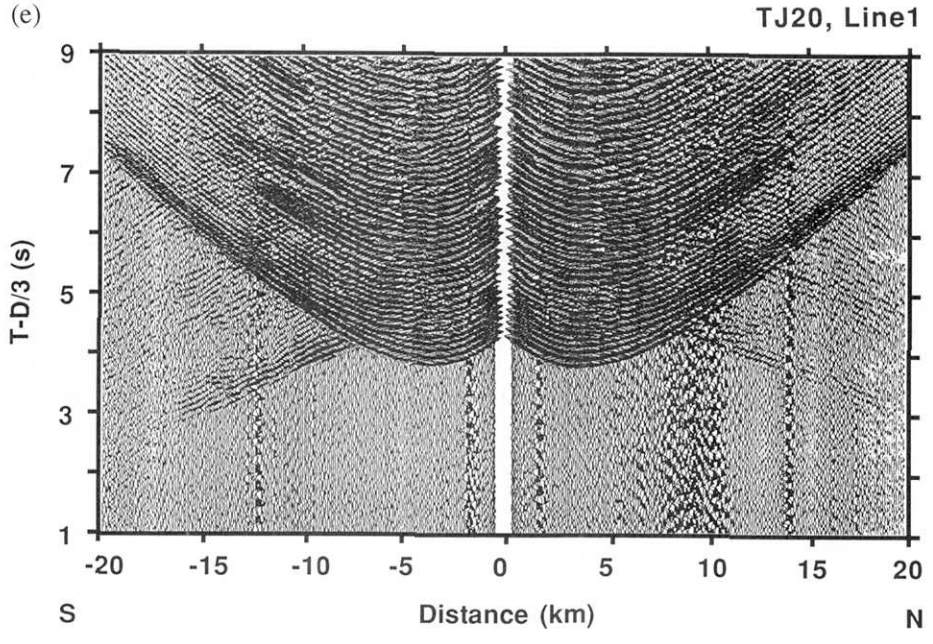
TJ20, Line1
T-D/3 (s)
9
7
5
3
1
-20
-15
-10
-5
0
5
10
15
20
S
Distance (km)
N

(f)

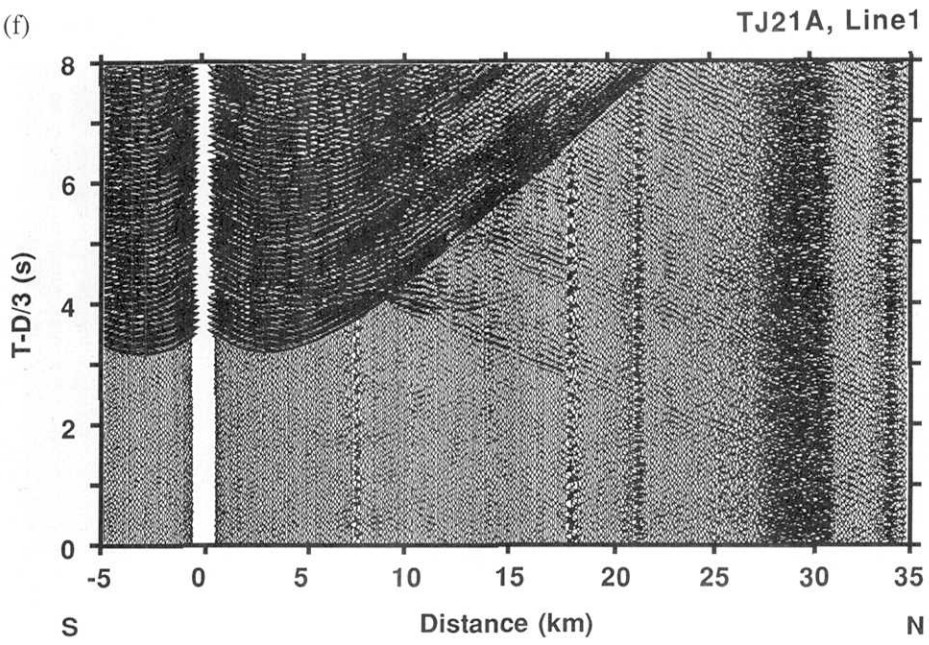
TJ21A, Line1
T-D/3 (s)
8
6
4
2
0
-5
0
5
10
15
20
25
30
35
S
Distance (km)
N

(g)

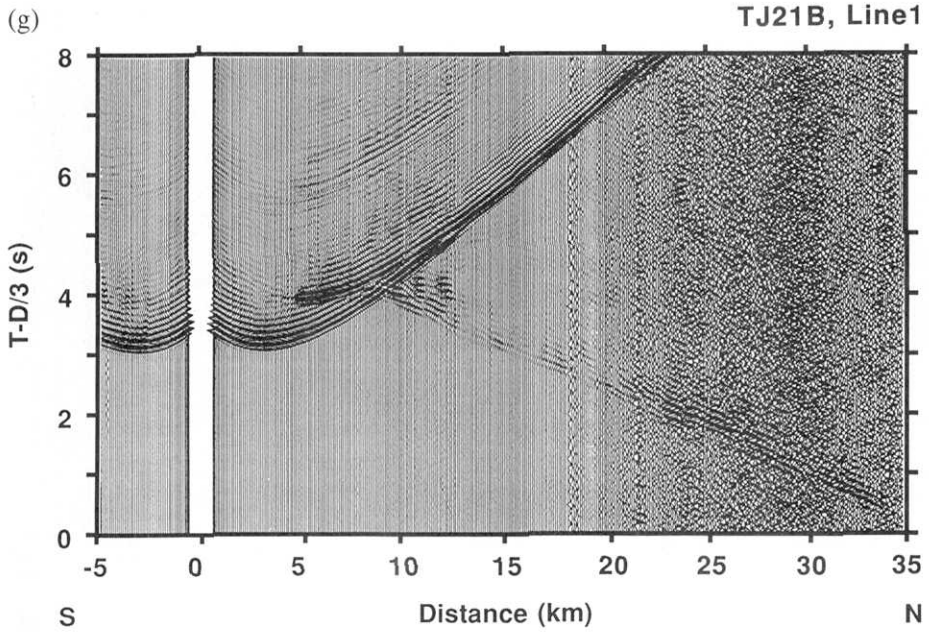
TJ21B, Line1
T-D/3 (s)
8
6
4
2
0
-5
0
5
10
15
20
25
30
35
S
Distance (km)
N

Record sections of OBSs on the Northeast Japan plate show a phase with a wave speed of 3 km/s in offset ranges from 5 to 8 km. We can see the phase later than a direct water wave arrival. Records of TJ4 and TJ5 indicate a phase of 5.0 km/s in ranges from 10 to 15 km (Figs. 9b, 9c). However, TJ7 and TJ18 have no records indicating the 5 km/s layer. Especially, records of TJ18 for Line 2 have the 3 km/s phase up to 20 km in the offset range suggesting that the 3 km/s layer is thick (Fig. 8). Generally, the apparent velocity of each phase is slower on the eastern side of the OBS than that on the western side, suggesting that each layer tilts downward to the east. The 3 km/s layer has a travel time curve which is convex upward, indicating the speed gradient with depth.

Records in the OBSs on the Pacific plate (e.g., TJ14, TJ15, TJ16) have a phase with a wave speed of 6 km/s in the range from 6 to 25 km, and of 8 km/s up to 45 km (Figs. 10d, 10e, 10f, 10g). The record section of TJ15 has a travel time curve that is symmetrical about the axis of the offset range, indicating horizontally homogeneous layering. The slightly convex travel time curve suggests the gradient of the wave speed with depth in the 6 km/s layer.

Records of OBSs in the very deep sea (TJ10, TJ11) have an asymmetrical pattern of travel time curves. Records of TJ10 have a phase with an apparent speed of 3 km/s in ranges from 14 km to 20 km. In the range from 14 to 20 km is a phase of 6 km/s. The record of TJ11 has a phase of 5.5 km/s on the eastern side and of 2.5 km/s on the western side (Fig. 10). The large apparent speed on the east is due to a steep seaward trench wall.

4.2. Analysis of OBS data

Travel times of refracted waves and reflected wide angle waves were picked

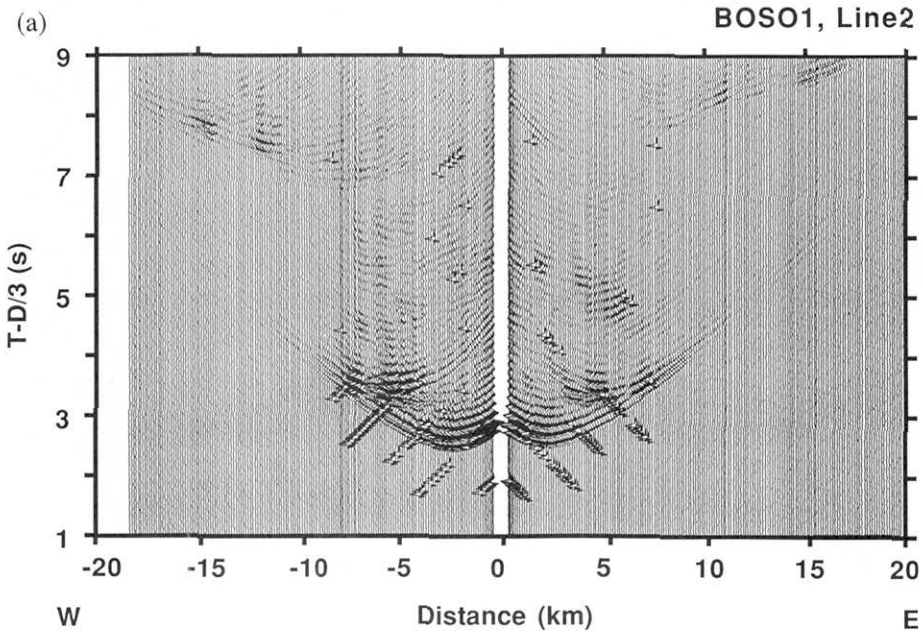

Fig. 8. Airgun signals recorded by OBSs on Line 2. Parameters for plotting are the same as in Fig. 7. (a) *BOSO1*. (b) TJ5. (c) TJ18.

(b)

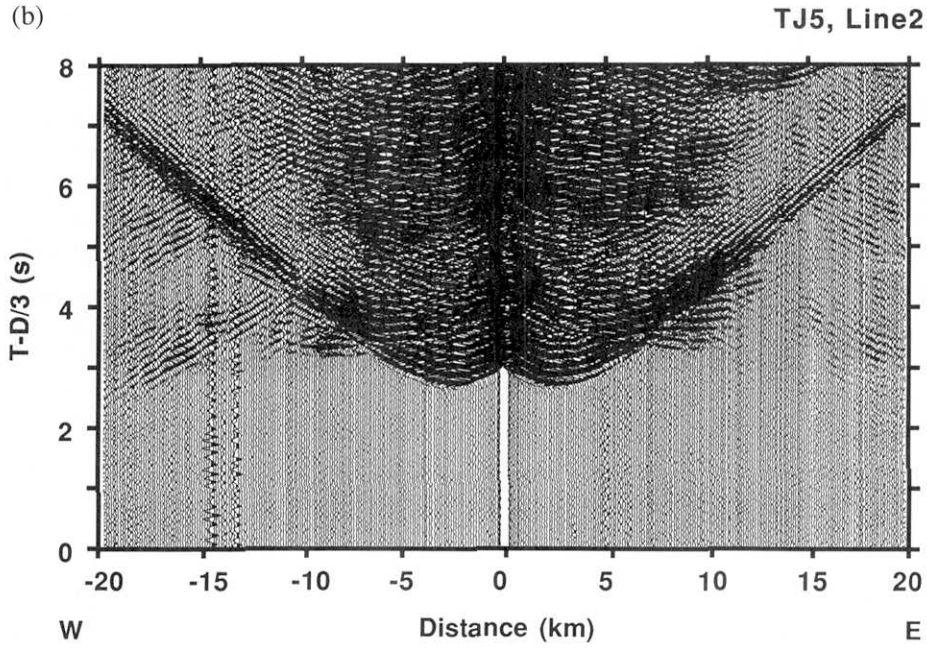
TJ5, Line2
T-D/3 (s)
8
6
4
2
0
-20
-15
-10
-5
0
5
10
15
20
W
Distance (km)
E

(c)

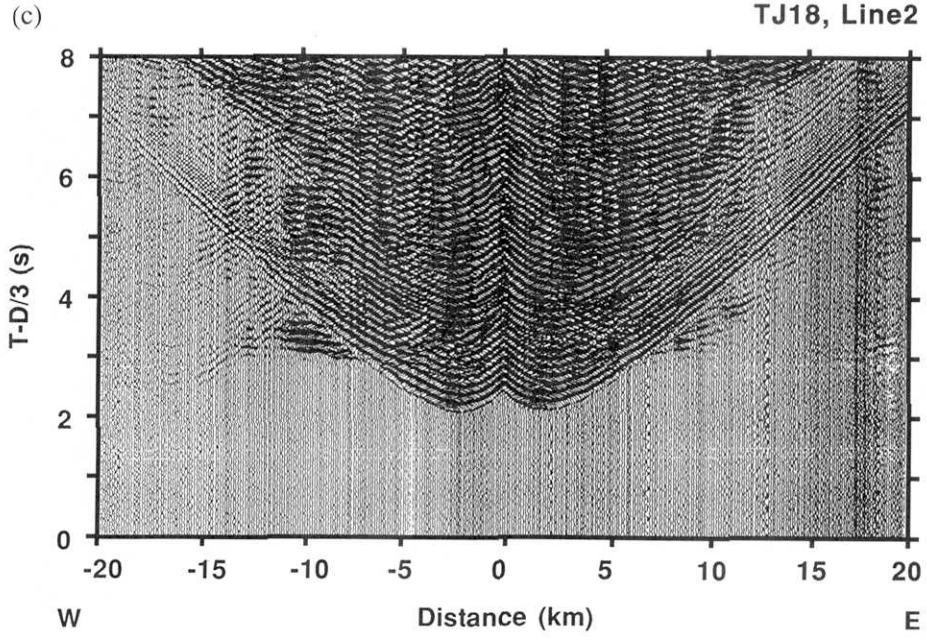
TJ18, Line2
T-D/3 (s)
8
6
4
2
0
-20
-15
-10
-5
0
5
10
15
20
W
Distance (km)
E

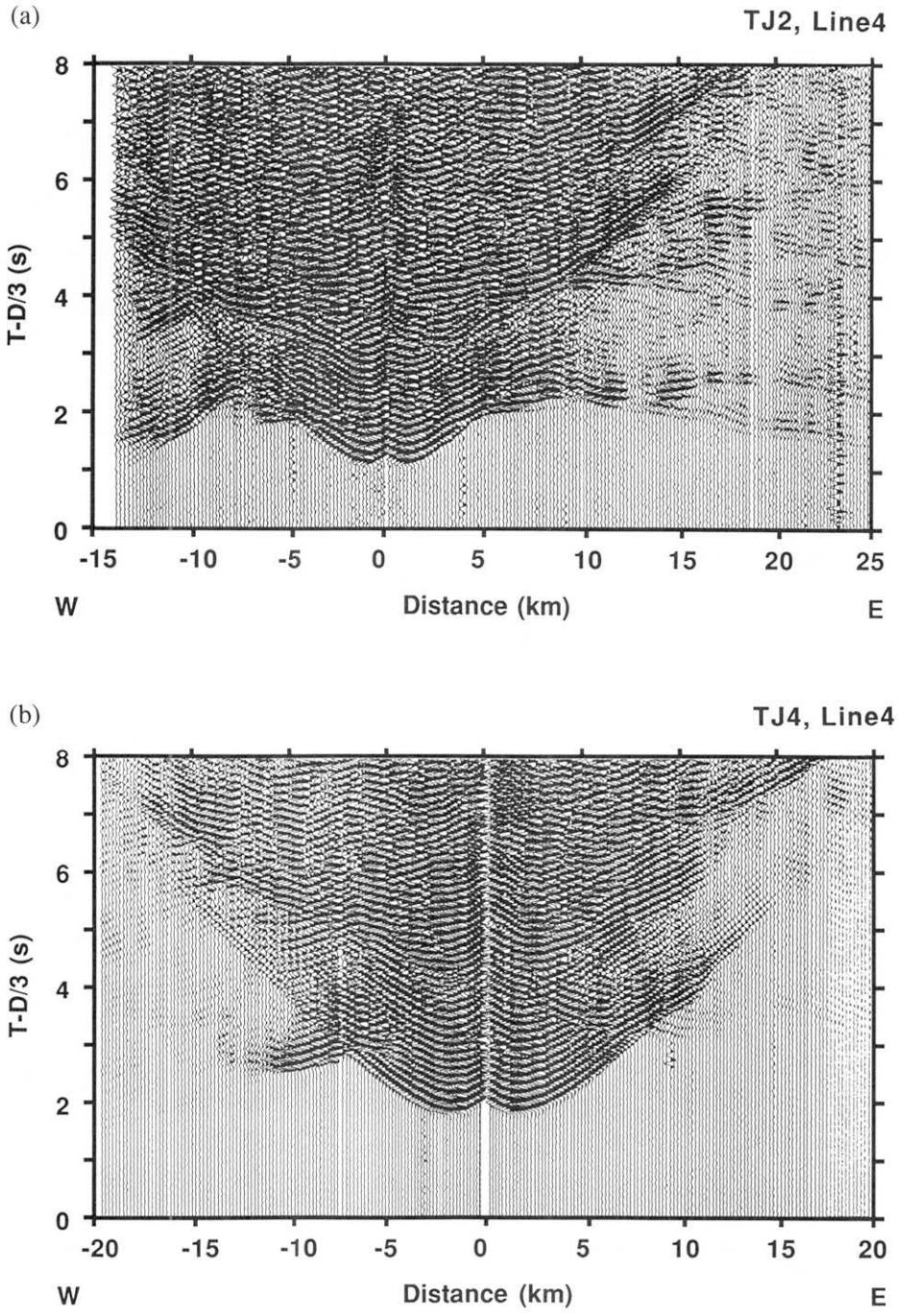

Fig. 9. Airgun signals recorded by OBSs on Line 4. Parameters for plotting are the same as in Fig. 7. (a) TJ2. (b) TJ4. (c) TJ5. (d) TJ6. (e) TJ7. (f) TJ8.

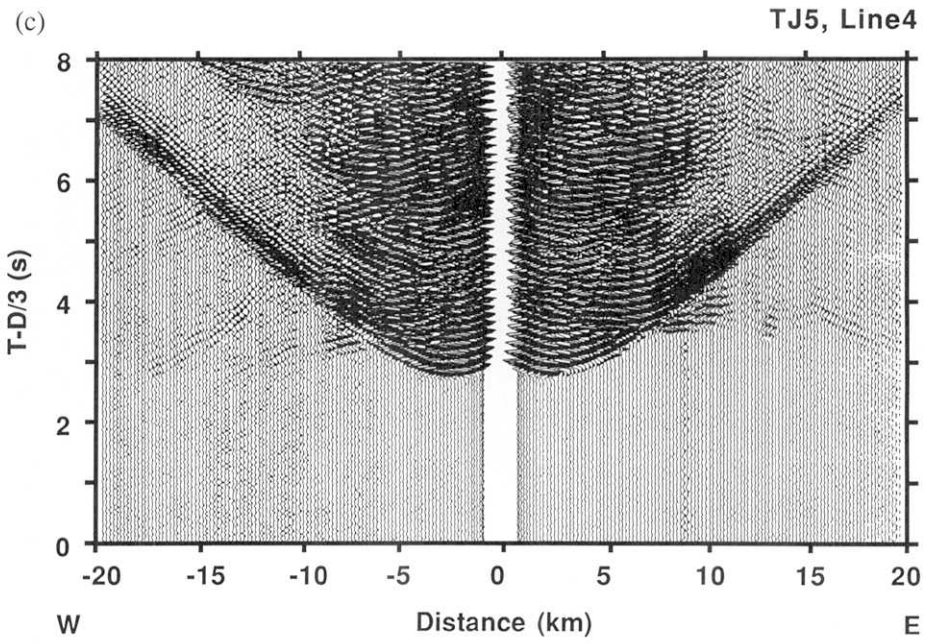
(c)
TJ5, Line4
T-D/3 (s)
8
6
4
2
0
-20
-15
-10
-5
0
5
10
15
20
W
Distance (km)
E

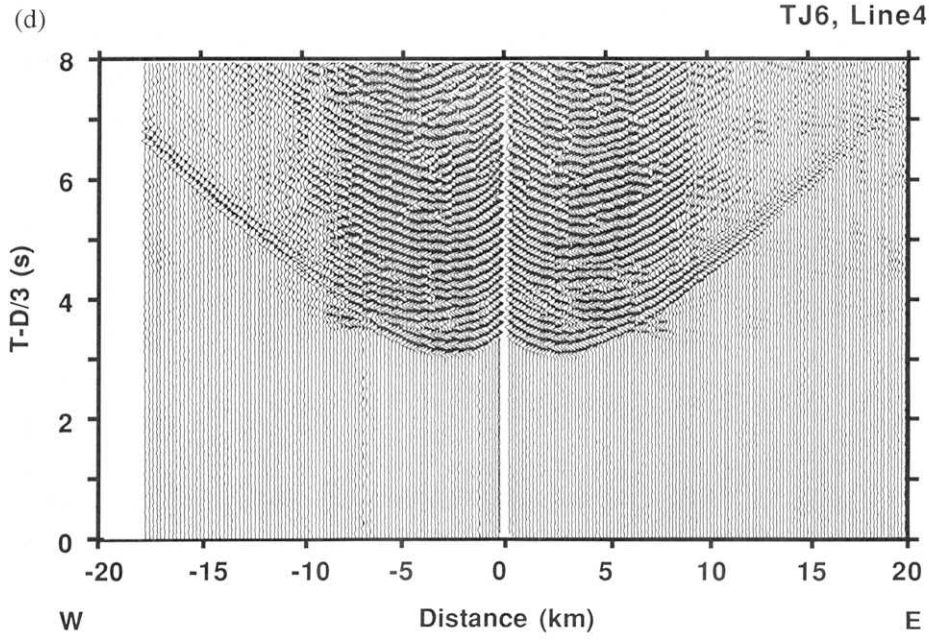
(d)
TJ6, Line4
T-D/3 (s)
8
6
4
2
0
-20
-15
-10
-5
0
5
10
15
20
W
Distance (km)
E

(e)

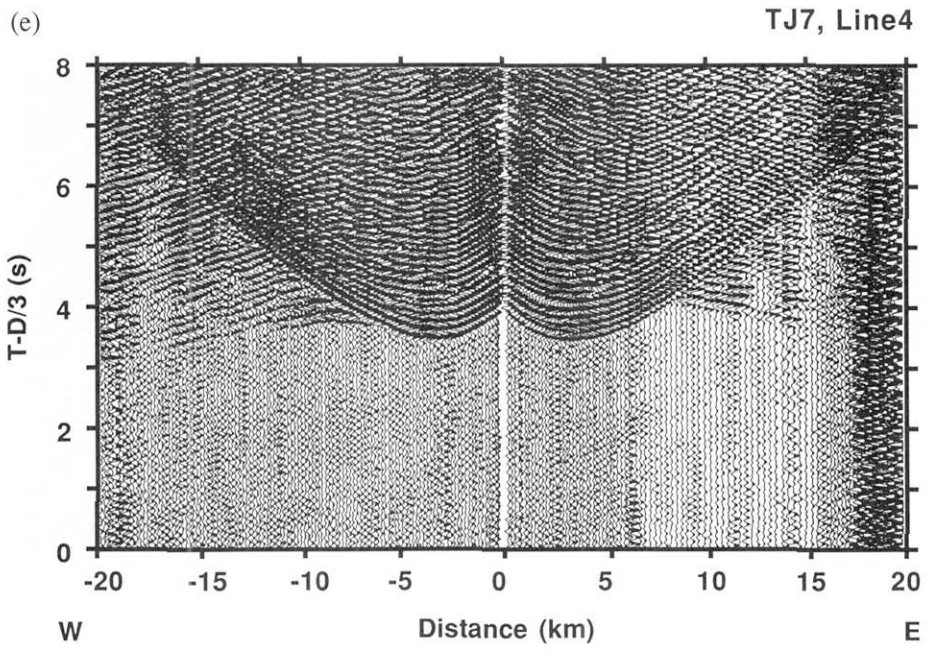
TJ7, Line4
T-D/3 (s)
8
6
4
2
0
-20
-15
-10
-5
0
5
10
15
20
W
Distance (km)
E

(f)

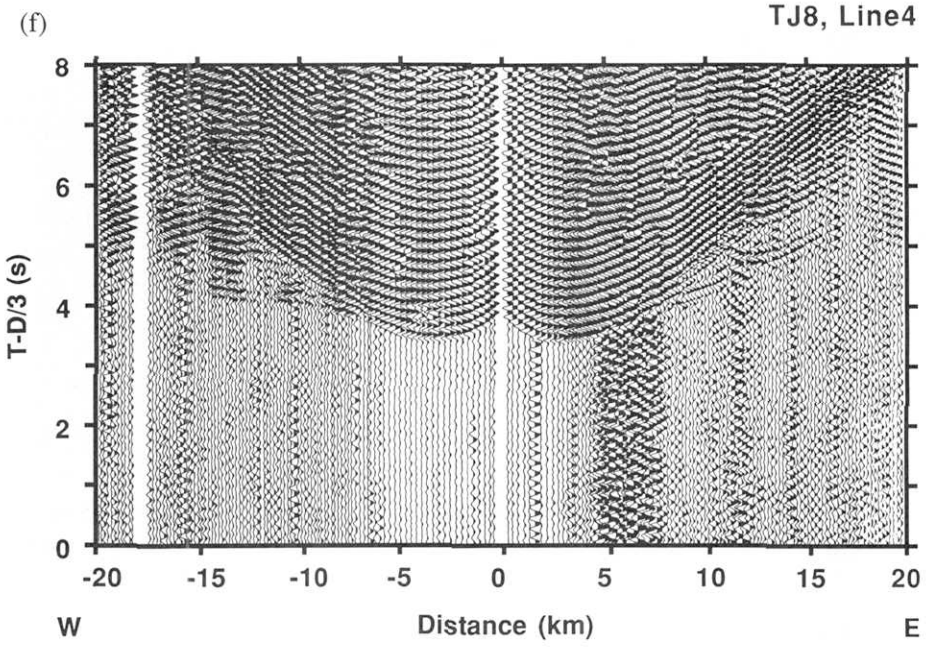
TJ8, Line4
T-D/3 (s)
8
6
4
2
0
-20
-15
-10
-5
0
5
10
15
20
W
Distance (km)
E

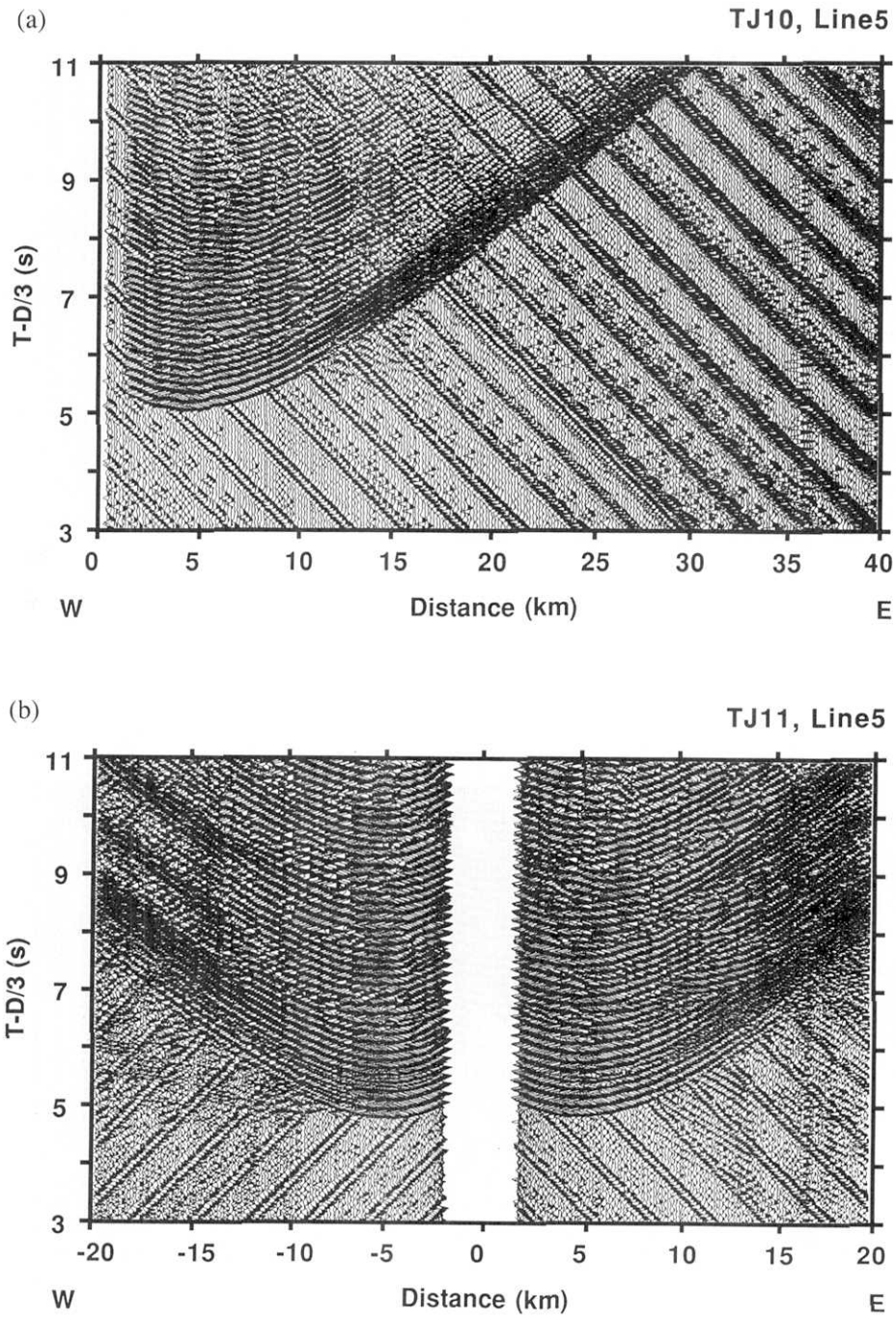

Fig. 10. Airgun signals recorded by OBSs on Line 5. Parameters for plotting are the same as in Fig. 7. (a) TJ10. (b) TJ11. (c) TJ13. (d) TJ14A. (e) TJ14B. (f) TJ15. (g) TJ16.

(c)

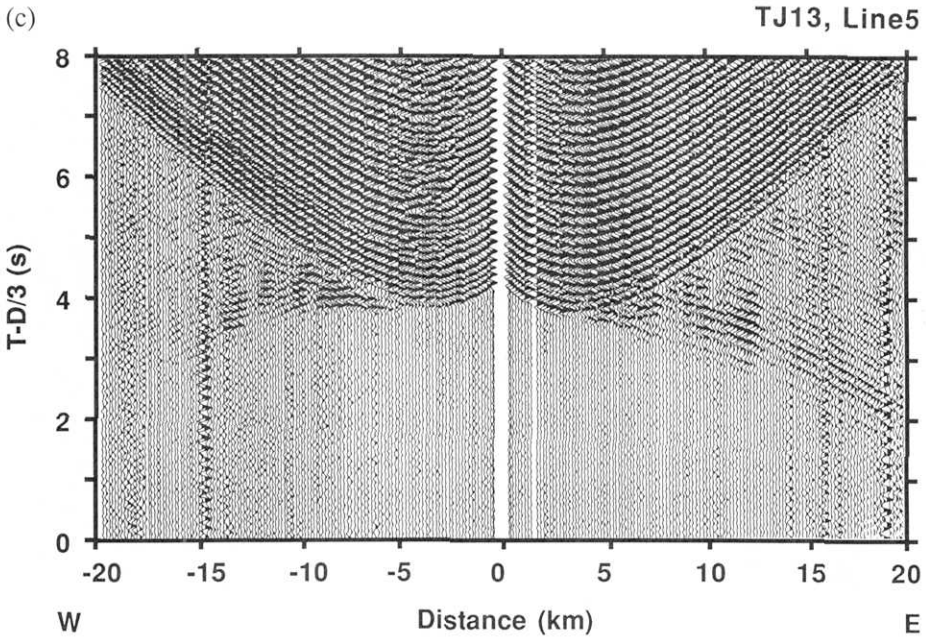
TJ13, Line5
T-D/3 (s)
8
6
4
2
0
-20
-15
-10
-5
0
5
10
15
20
W
Distance (km)
E

(d)

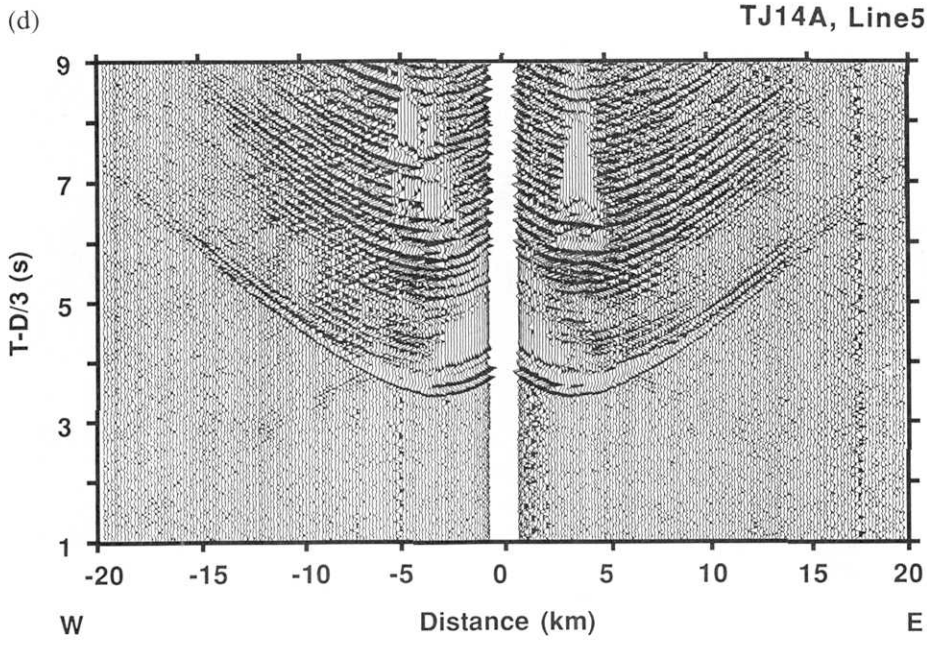
TJ14A, Line5
T-D/3 (s)
9
7
5
3
1
-20
-15
-10
-5
0
5
10
15
20
W
Distance (km)
E

(e)

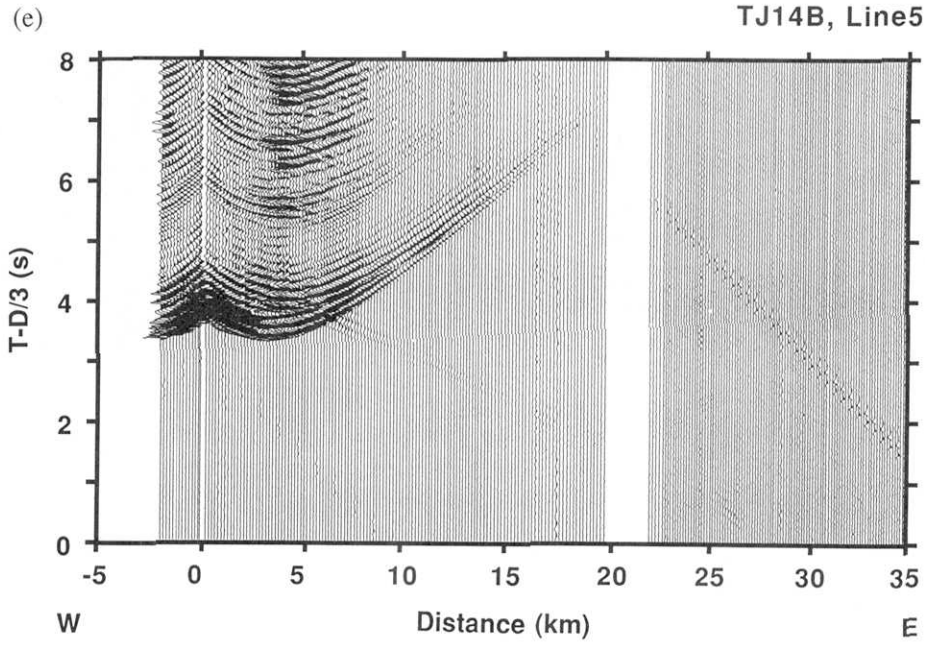
TJ14B, Line5
T-D/3 (s)
8
6
4
2
0
-5
0
5
10
15
20
25
30
35
W
Distance (km)
E

(f)

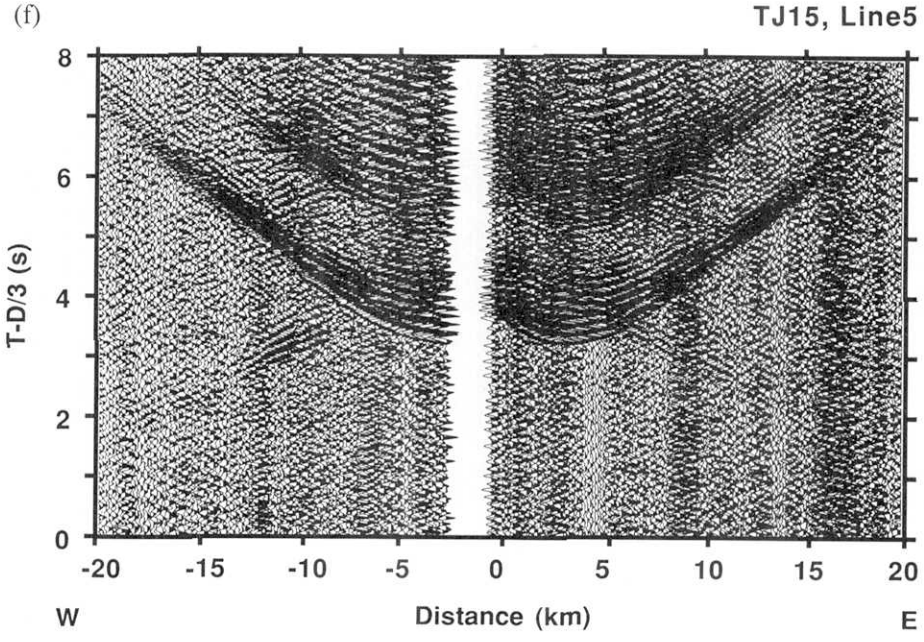
TJ15, Line5
T-D/3 (s)
8
6
4
2
0
-20
-15
-10
-5
0
5
10
15
20
W
Distance (km)
E

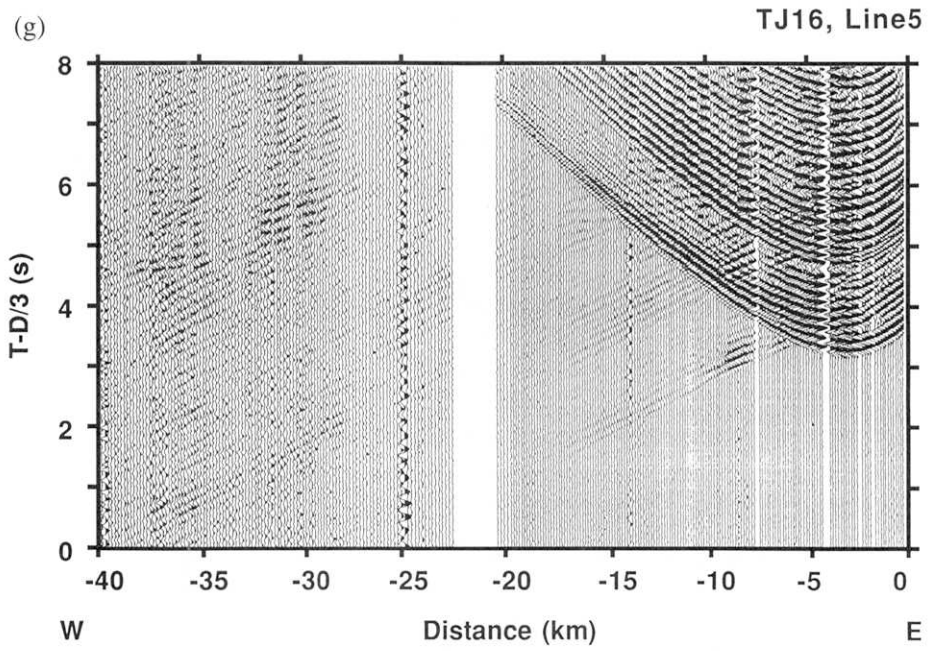

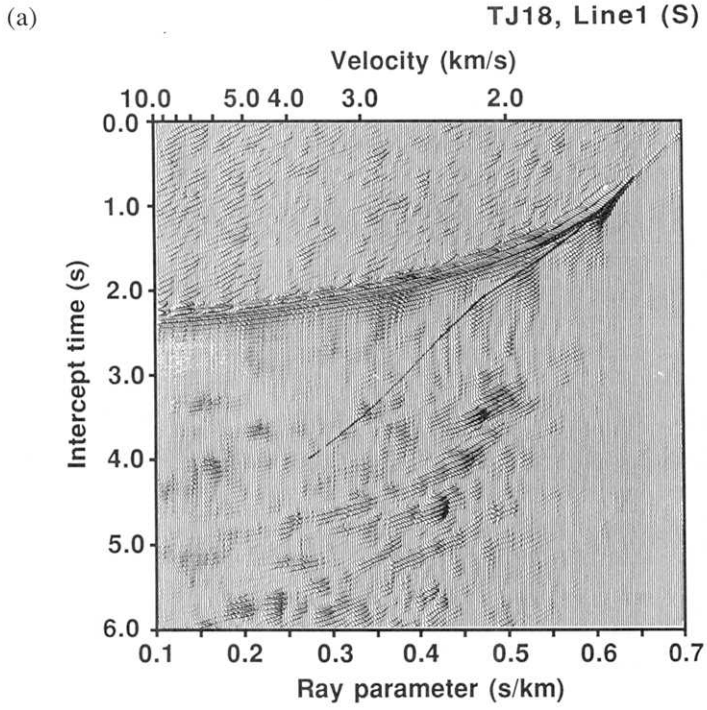

Fig. 11. Example of the τ-p transform of airgun signal recorded by OBSs. τ-p seismograms of Line 1 recorded by TJ18 and TJ21 are shown. The vertical component records of geophone with low gain amplification are processed within an offset range of 10 km. A curve indicates a picked trajectory of principal arrivals. (a) South side of TJ18. (b) North side of TJ18. (c) North side of TJ21A.

(b)

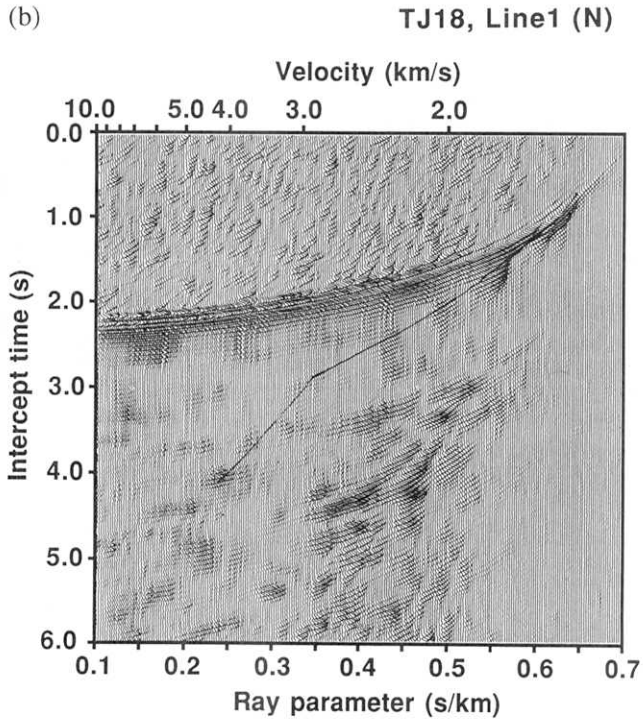
TJ18, Line1 (N)
Velocity (km/s)
10.0
5.0
4.0
3.0
2.0
0.0
1.0
2.0
3.0
4.0
5.0
6.0
Intercept time (s)
0.1
0.2
0.3
0.4
0.5
0.6
0.7
Ray parameter (s/km)

(c)

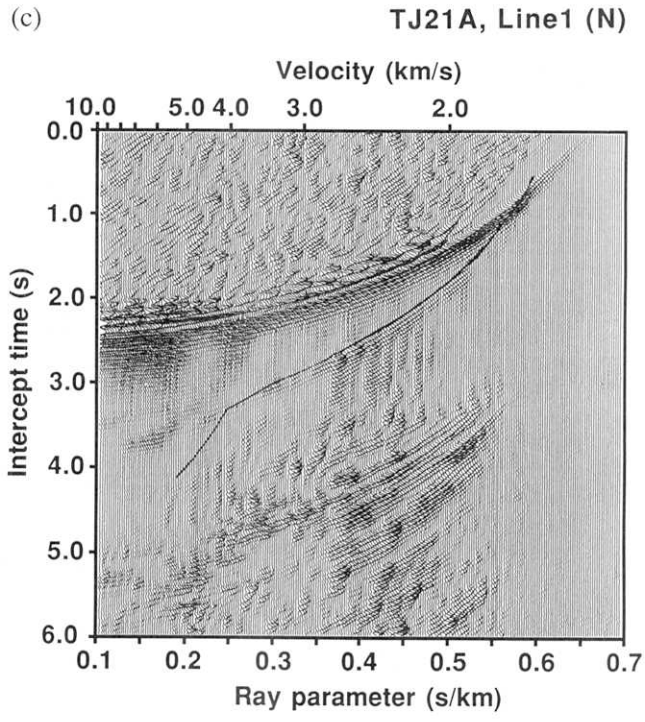
TJ21A, Line1 (N)
Velocity (km/s)
10.0
5.0
4.0
3.0
2.0
0.0
1.0
2.0
3.0
4.0
5.0
6.0
Intercept time (s)
0.1
0.2
0.3
0.4
0.5
0.6
0.7
Ray parameter (s/km)

manually from transcribed record sections of OBSs. Also, the record section in the travel time – offset distance (t–x) domain was transformed to the intercept time – ray parameter (τ–p) domain (SHINOHARA *et al.*, 1993). We show some examples of the τ–p transform of the record section in Fig. 11. We calculated semblance s_{ij} for each pair of (τ_i, p_j) from seismogram $f(t, x)$ in the t–x domain as:

$$s(\tau_i,\ p_j)=\frac{\sum_W\left(\sum_{k=1}^{N} f(\tau_i+p_j x_k)\right)^2}{N\sum_W\sum_{k=1}^{N}(f(\tau_i+p_j x_k))^2},$$

where W is a time window with a center of τ_i and N is the number of traces in the t–x domain (NEIDELL and TANER, 1971). We used the 0.1 s long window for the following calculation. The increment of p_j (Δp_j) is 0.05 s/km. In order to determine the shallower structure of the crust, we applied the t-sum inversion method (DIEBOLD and STOFFA, 1981) to the manually picked τ–p trajectory. We show some examples of the results of the inversion in Fig. 12, in which crustal structures among different sites are compared. Because we assumed a horizontally homogeneous model in the inversion, we basically obtained two different crustal models for a split profile. We depicted them independently with different symbols to see how they differ each other. For example, the wave speed depth profile determined from the westward shooting of TJ5 on Line 4 has a higher P-wave speed than that from eastward shooting. The difference is due to eastward down dipping of the layer along Line 4.

We then averaged two models for one OBS to derive one-dimensional wave speed profile with depth. All the analyzed profiles are summarized in columnar charts with topography and clear reflector seen in the SCS reflection data (Fig. 13). We can see a good correlation between the model derived from the refraction data of OBSs and that from the reflection data.

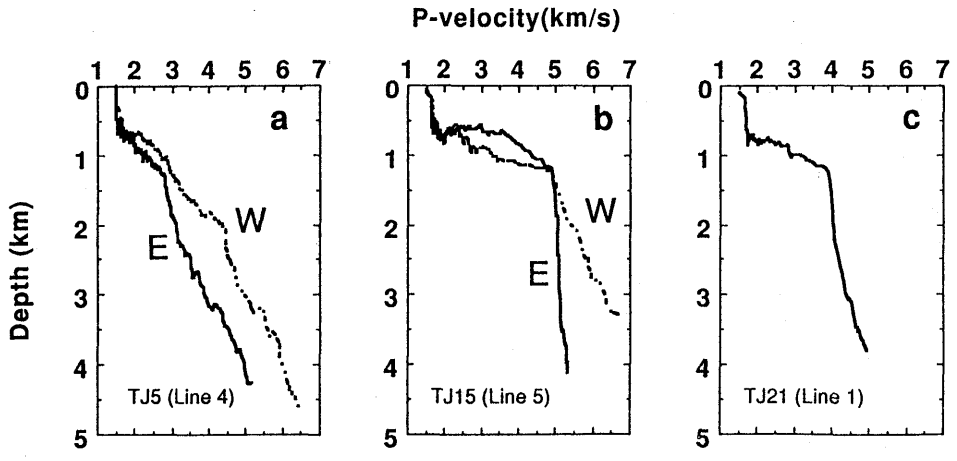

Fig. 12. Example of wave speed depth profiles determined by the τ-sum inversion using τ–p data as shown in Fig. 11. (a) TJ5 on Line 4. Solid line labeled E denotes model derived from eastward shot of the OBS. Dashed line labeled W denotes that from westward shot. (b) TJ15 on Line 5. (c) TJ21A on Line 1. Data are from northward shot.

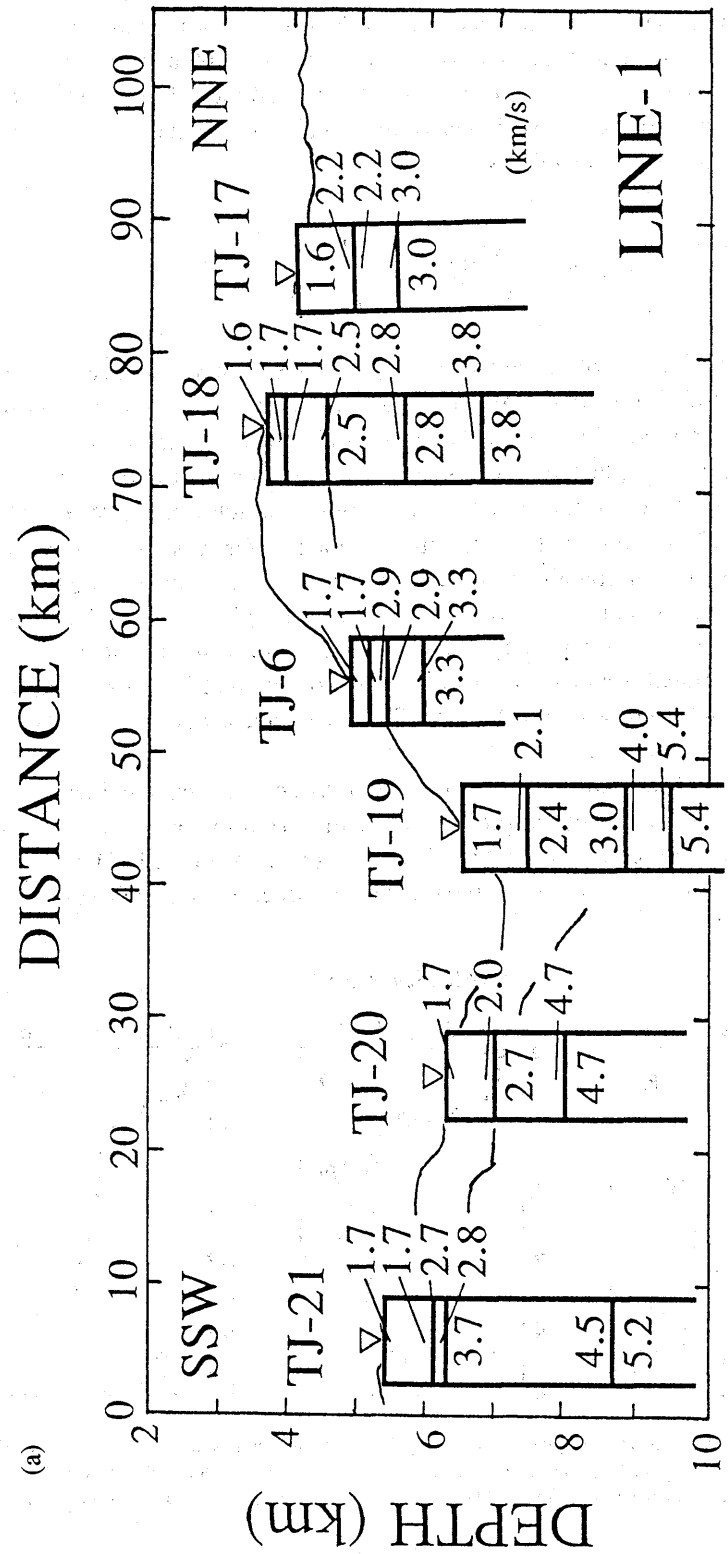

Fig. 13. Summary of one-dimensional crustal structures. Each model is derived from individual OBS data. Topography and clear reflectors interpreted from the SCS profiles are also shown. Numerals are P wave speeds in km/s. (a) Line 1. (b) Line 2. (c) Line 4. (d) Line 5.

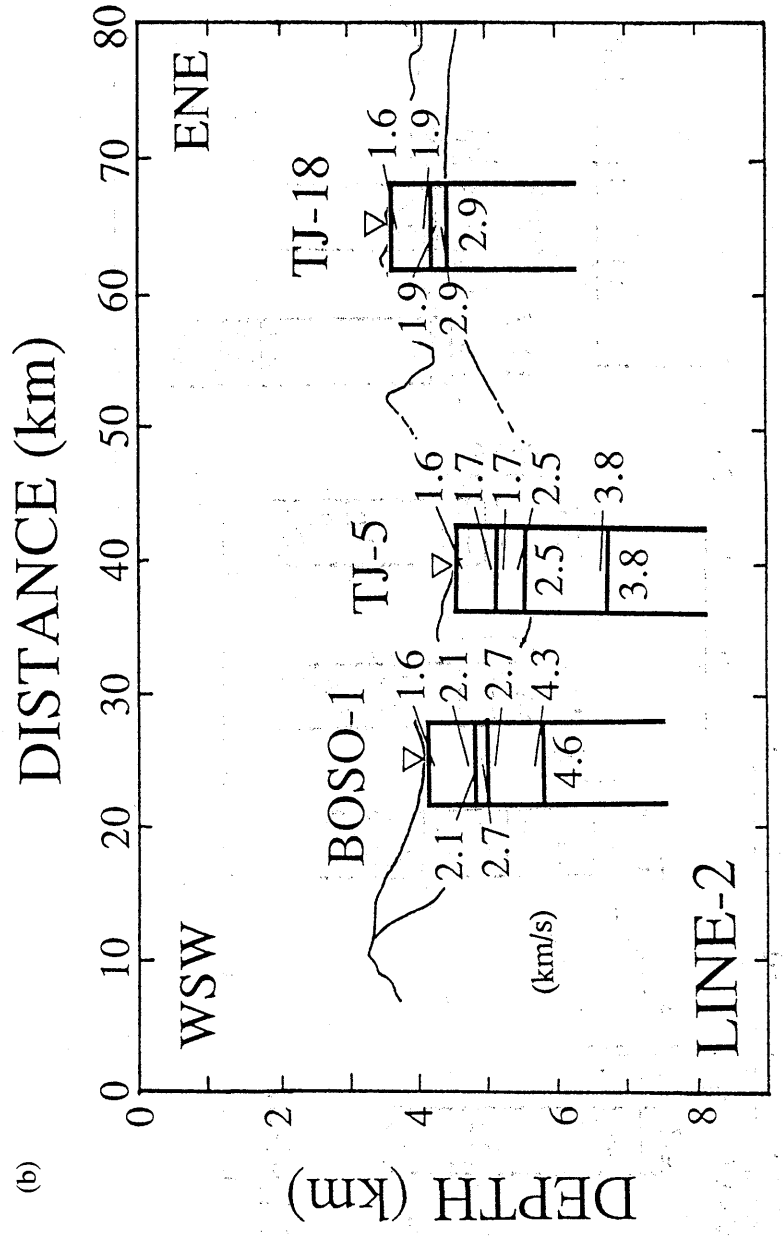
(b)
DISTANCE (km)
0
10
20
30
40
50
60
70
80
WSW
ENE
BOSO-1
TJ-5
TJ-18
1.6
2.1
2.7
4.3
4.6
1.6
1.7
1.7
2.5
2.5
3.8
3.8
1.6
1.9
1.9
2.9
2.9
(km/s)
DEPTH (km)
0
2
4
6
8
LINE-2

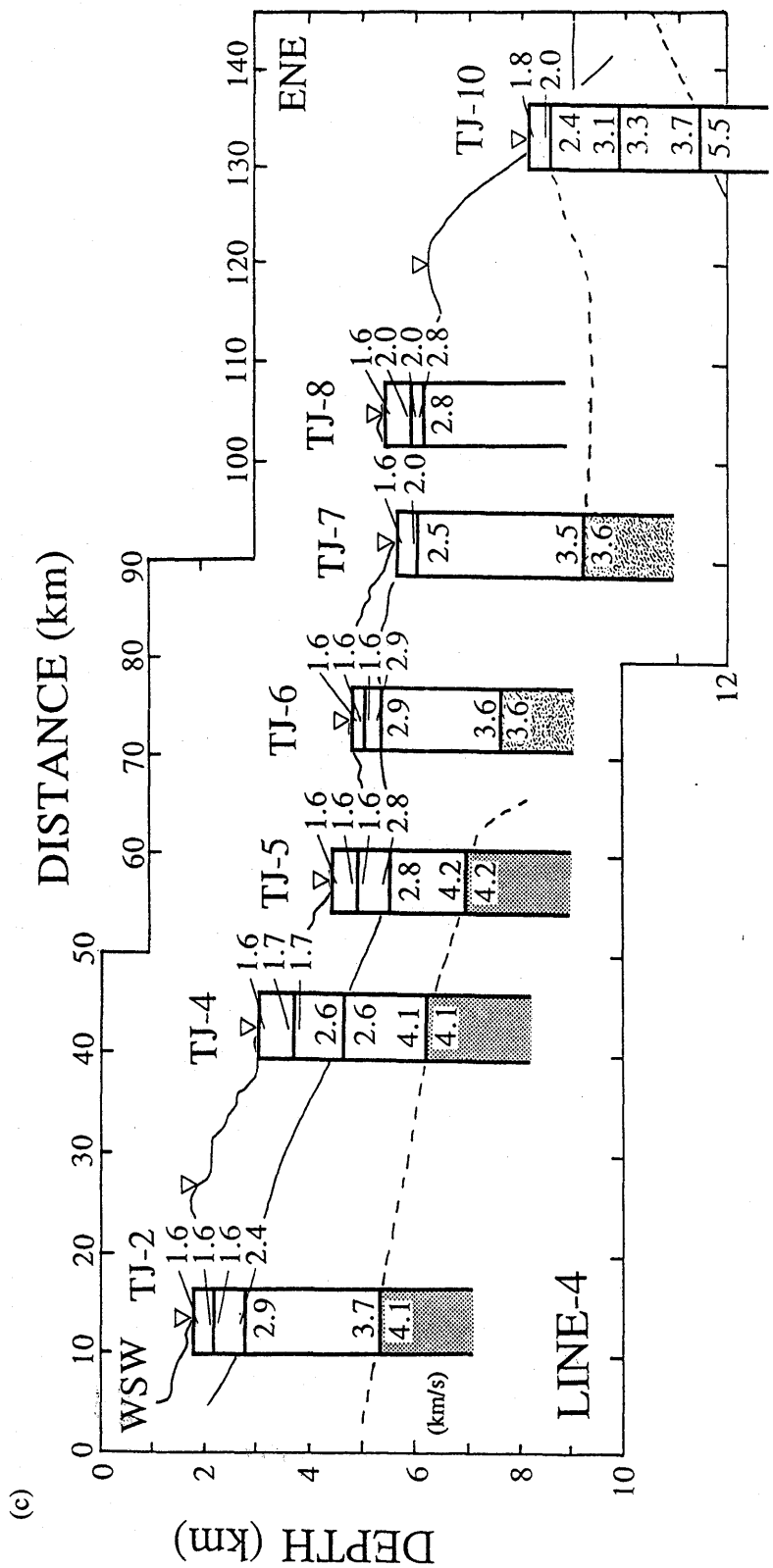
WSW
ENE
LINE-4
DISTANCE (km)
DEPTH (km)
(km/s)
TJ-2
TJ-4
TJ-5
TJ-6
TJ-7
TJ-8
TJ-10
0
10
20
30
40
50
60
70
80
90
100
110
120
130
140
0
2
4
6
8
10
12

(c)

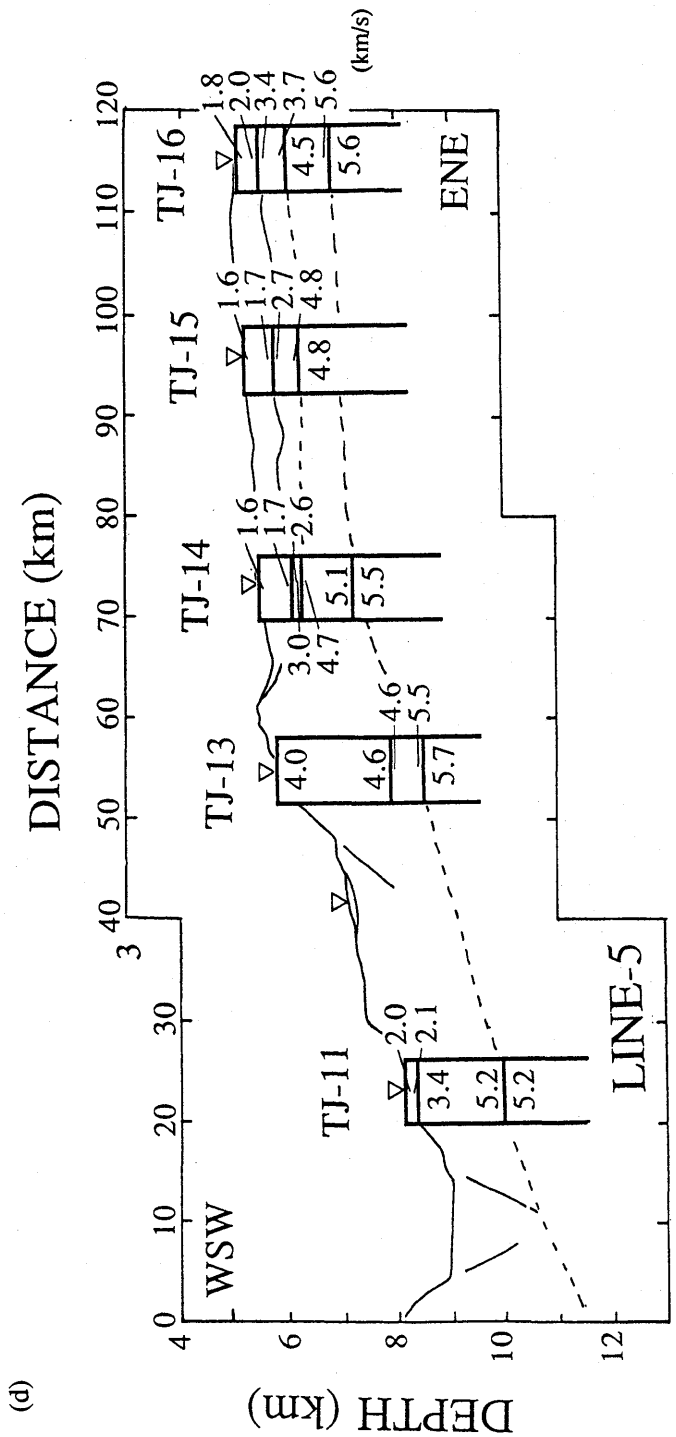
(d)
DEPTH (km)
DISTANCE (km)
WSW
ENE
LINE-5
TJ-11
TJ-13
TJ-14
TJ-15
TJ-16
(km/s)
1.8
2.0
3.4
3.7
5.6
4.5
5.6
1.6
1.7
2.7
4.8
4.8
1.6
1.7
2.6
3.0
4.7
5.1
5.5
4.0
4.6
4.6
5.5
5.7
2.0
2.1
3.4
5.2
5.2

5. Discussion

5.1. Thickness of sedimentary layer

Both the single channel reflection data and refraction data of OBSs indicate clear differences in sedimentary layer structure among sites (Fig. 13): The layer thickness on the oceanic side is 1 km beneath TJ15 and on the continental slope 3 km beneath TJ14 and TJ5. Along the E-W main profile (Lines 4 and 5) we can see the maximum thickness around TJ7, where the sediment is 4 km thick. Although the acoustic basement beneath the inner trench wall of the Izu-Bonin Trench is not clearly seen in the reflection data, the refraction data from the OBS definitely document a thick pile of sediment there.

5.2. *P*-wave speed in the sediment

The uppermost sedimentary layer has a *P*-wave speed of 1.6 km/s, which is very close to the *P*-wave speed in the water layer. The layer is widely found beneath both the oceanic side and the continental side of the trench axis. It corresponds to the uppermost transparent layer in the acoustic stratigraphy. We think that it consists of unconsolidated sediment. The layer thickness varies from site to site, but generally it is within the range of 200–300 m. The wave speed gradient with depth in the layer is smaller on the oceanic side than that on the continental side: 0.32 s^{-1} beneath TJ15 and 0.65 s^{-1} beneath TJ5.

Below the uppermost transparent layer is the layer in which the *P*-wave speed rapidly increases with depth. On the oceanic side the layer has a wave speed gradient of 4.8 s^{-1} (TJ15) and on the continental side the gradient is smaller: 0.8 s^{-1} is observed at TJ5.

5.3. *P*-wave speed in the basement layer

Since both reflection and refraction data are available, we can correlate the acoustic stratigraphy with the *P*-wave speed to identify the lithology of the layer. First, we can recognize that the transparent layer of Pac 1 corresponds to unconsolidated sediment in which the *P*-wave speed gradient with depth is small. The acoustic characteristics suggest that this layer is much more homogeneous than the lower layers. The interface between Pac 1 and Pac 2 forms an acoustic basement, but the *P*-wave speed indicates that the uppermost part of Pac 2 is also a sedimentary layer. The rapid increase of the *P*-wave speed is indicative of compaction of the sediment. It is clear from the reflection and the refraction data (Fig. 13) that the acoustic basement does not correspond to the top of igneous crust, while the *P*-wave speed of around 5 km/s is typical in the oceanic crust.

Similarly, on Line 4 of the continental slope, the *P*-wave speeds indicate that the layers which we referred to as NJ 1, NJ 2, and NJ 3 in the acoustic stratigraphy have *P*-wave speeds slower than that in the basement layer. The speed versus depth profiles increase gradually with depth from 1.6 km/s to 4 km/s. These observations indicate that the top 3–4 km of the crust consists of a series of sedimentary layers (TJ2). The bottom of the sediment is more than 4 km below the sea bottom. The maximum *P*-wave speed derived from the airgun-OBS data (TJ2, TJ4, TJ5) is around 5.0 km/s, which may correspond to that of the basement rock (Fig. 12).

5.4. Philippine Sea plate below Northeast Japan plate

Beneath TJ7 is the thickest and slowest sedimentary layer in the studied area. Recently, IWABUCHI *et al.* (1990) reports the detailed structure of the upper crust using multichannel reflection data in the vicinity of the triple junction. According to their interpretation, the eastern edge of the Philippine Sea plate is exposed just east of the Daito spur. Beneath TJ7 are both the Philippine Sea and the Pacific plates below the Northeast Japan plate: the boundary between the Northeast Japan and the Philippine Sea plates is approximately 3 km below the sea bottom. If this is the case, the 3.6 km/s layer of TJ7 belongs to the Philippine Sea plate. Our OBS data show no clear difference in *P*-wave gradient with depth between those above and below the boundary. Moreover, the *P*-wave speed of 3.6 km/s is slower as compared with 4.1 km/s at 3 km depth beneath other OBSs on the continental slope. So we think that even if the plate boundary between the two plates exists, the topmost part of the lower plate (Philippine Sea plate) is heavily deformed or fractured to decrease the *P*-wave speed.

6. Conclusion

We conducted airgun-OBS profiling using both reflection and refraction methods. Twenty-two ocean bottom seismographs were deployed in an array to study the crustal structure in the vicinity of the triple junction. The profiling consisted of four lines which covered the Pacific, the Northeast Japan, and the Philippine Sea plates. We obtained a detailed structure of the shallow crust including the sedimentary layer and the basement layer. The seismic structure varies considerably along the profiles. Especially, the difference of the structure in the vertical gradient of *P*-wave speed is evident between the oceanic side and the continental side: beneath TJ15 on the Pacific plate are a vertically homogeneous unconsolidated sediment (0.32 s^{-1} of vertical wave speed gradient) and a consolidated sediment where the *P*-wave speed increases quite rapidly (4.8 s^{-1}), while beneath TJ5 on the Northeast Japan plate the gradient is 0.65 s^{-1} in the topmost and 0.8 s^{-1} in the lower part of the sediment.

The *P*-wave speed in the basement layer also varies along the profile. Beneath the continental slope, where the Northeast Japan is supposed to be underlain by the Philippine Sea plates, the wave speed increases gradually with depth without any abrupt changes. The structure in the shallow crust suggests that the topmost part of the Philippine Sea plate underlying the Northeast Japan plate is considerably deformed or fractured to have no clear boundary between the plates.

Acknowledgments

We thank the Captain, officers and crew of the *R/V Kaikomaru No. 5* for their help in operation of the seismic experiment. We express our thanks to the shipboard scientific party of the 1989 DELP Cruise in the Off-Boso triple Junction. We owe very much to Dr. T. Ouchi for his help in operation of OBSs. Three very deep OBSs were deployed from the *R/V Hakuhomaru*. We are grateful to Prof. K. Suyehiro on board, with whom

stimulus discussion we made. Discussion with Dr. H. Tokuyama on interpretation of the SCS data was very helpful. We thank students of Chiba University for installation of land stations.

The permanent OBSs off the Boso Peninsula were operated by the Japan Meteorological Agency. Many people from JMA were very helpful for providing us continuous records during the experiment.

References

BABA, H., N. DEN, S. IIZUKA and Y. MISAWA, 1988, Explosion seismic obsevations in and around Suruga Bay by the new pop-up type ocean bottom seismometers. *Bull. Inst. Oceanic Res. & Develop., Tokai Univ.*, **9**, 45–53.

DIEBOLD, J.B. and P.L. STOFFA, 1981, The traveltime equation, tau-p mapping, and inversion of common midpoint data, *Geophysics*, **46**, 238–254.

FUJISAWA, I., S. TATEYAMA and J. FUNASAKI, 1986, Permanent Ocean-bottom earthquake and tsunami observation system off the Boso Peninsula, *Weather Serve. Bull., Jpn. Meteor. Agency*, **53**, 127–166.

HIRATA, N. and M. MATSU'URA, 1987, Maximum-likelihood estimation of hypocenter with origin time eliminated using nonlinear inversion technique, *Phys. Earth Plant. Int.*, **47**, 50–61.

HIRATA, N., T. ASANUMA, T. FUJIWARA, T. KAMATA and H. KINOSHITA, 1990, The 1989 geophysical experiment in and off the Boso Peninsula for the study of the crustal structure around the trench-trench-trench triple junction, *Ann. Rep. Mar. Ecosystems Res. Ctr., Chiba Univ.*, **10**, 75–82.

IWABUCHI, Y., A. ASADA and Y. KATO, 1990, Multi-channel seismic reflection survey around the plate triple junction off Boso Peninsula, *J. Jpn. Soc. Marine Surv. Tech.*, *2*, 29–38.

IWASAKI, T., H. SHIOBARA, A. NISHIZAWA, T. KANAZAWA, K. SUYEHIRO, N. HIRATA, T. URABE and H. SHIMAMURA, 1989, A detailed subduction structure in the Kuril trench deduced from ocean bottom seismographic refraction studies, *Tectonophysics*, **165**, 315–336.

IWASAKI, T., N. HIRATA, T. KANAZAWA, J. MELLES, K. SUYEHIRO, T. URABE, L. MOLLER, J. MAKRIS and H. SHIMAMURA, 1990, Crustal and upper mantle structure in the Ryukyu Island Arc deduced from deep seismic sounding, *geophys. J. Int.*, **102**, 631–651.

JACKSON, D.D. and M. MATSU'URA, 1985, A Bayesian approach to nonlinear inversion, *J. Geophys. Res.*, **90**, 581–591.

KANAZAWA, T. and Y. KAIHO, 1990, Ocean bottom seismometer for deep sea observation near trench axis (in Japanese), *Prog. Abst. seismol. Soc., Japan*, **1**, 21.

KATO, S., T. NAGAI, M. TAMAKI, T. KONDO, Y. TOMIYASU, G. KATO, K. MUNEDA and A. ASADA, 1985, Submarine topography of the eastern Sagami Trough to the triple junction, *Rep. Hydrogr. Res.*, **20**, 1–24.

KINOSHITA, H., Y. HAMANO and A. UCHIYAMA, 1986, Studies on the detailed crustal structure of the trench-trench-trench triple junction off southeast Japan, *Tectonophysics*, **132**, 79–87.

LUDWIG, W., J. EWING, S. MURAUCHI, N. DEN, S. ASANO, H. HOTTA, M. HAYAKAWA, T. ASANUMA and I. NOGUCHI, 1966, Sediments and structure of the Japan Trench, *J. Geophys. Res.*, **71**, 2121–2137.

MATSUDA, N., T. FUJII and H. KINOSHITA, 1986, A pop-up type ocean bottom seismograph with geophones and a hydrophone for the study of crustal structures (in Japanese), *Prog. Abst. seismol. Soc., Japan*, **2**, 241.

MCKENZIE, D.P. and W.J. MORGAN, 1969, Evolution of triple junctions, *Nature*, **224**, 125–133.

NAGUMO, S., J. KASAHARA, S. KORESAWA and H. MURAKAMI, 1982, Acoustic release ocean-bottom seismometer (ERI-AR81), *Bull. Earthq. Res. Inst., Univ., Tokyo*, **57**, 125–132.

NEIDELL, N.S. and M.T. TANER, 1971, Semblance and other coherency measures for multichannel data, *Geophysics*, **36**, 483–497.

OGAWA, Y., T. SENO, H. TOKUYAMA, H. AKIYOSHI, K. FUJIOKA and H. TANIGUCHI, 1989, Structure and development of the Sagami Trough and the Boso triple junction, *Tectonophysics*, **160**, 135–150.

RENARD, V., K. NAKAMURA, J. ANGELIER, J. AZEMA, J. BOURGOIS, C. DEPLUS, K. FUJIOKA, Y. HAMANO, P. HUCHON, H. KINOSHITA, P. LABAUME, Y. OGAWA, T. SENO, A. TAKEUCHI, M. TANAHASHI, A. UCHIYAMA and J.-L. VIGNERESSE, 1987, Trench triple junction off central Japan – preliminary results of French-Japanese 1984 Kaiko cruise, Leg 2, *Earth and Planetary Science Letters*, **83**, 243–256.

SENO, T., Y. OGAWA, H. TOKUYAMA, E. NISHIYAMA and A. TAIRA, 1989, Tectonic evolution of the triple junction off central Honshu for the past 1 million years, *Tectonophysics*, **160**, 91–116.

SHINOHARA, M., T. AMISHIKI, R. HINO, N. HIRATA and H. KINOSHITA, 1989, Digital data acquisition system for sin-

gle channel reflection experiment using a micro computer, *Prog. Abst. seismol. Soc., Japan,* **2,** 259.

SHINOHARA, M., N. HIRATA and N. TAKAHASHI, 1993, High resolution velocity analysis of ocean bottom seismometer data by the τ–p method, *Mar. Geophys. Res.*, **15,** in press.

TAIRA, A. and SHIPBOARD SCIENTIFIC PARTY, 1988, Preliminary report of the Hakuho Maru cruise KH 86-5, *Ocean Res. Inst., Univ. Tokyo,* 284 pp.

URABE, T. and N. HIRATA, 1984, A playback system for long term analogue tape recordings of ocean bottom seismographs, *Zisin (J. seism. Soc. Jpn),* **37,** 633–645.

YAMADA, T., T. ASADA and H. SHIMAMURA, 1981, A pop-up ocean bottom seismograph, *Prog. Abst. seismol. Soc., Japan,* **2,** 126.

1989年度DELP海溝三重会合点海域調査研究航海報告 第二部：房総沖海溝三重会合点付近の上部地殻構造

平田　直[3]・高橋成実・網敷俊志[1]
篠原雅尚[2]・木下肇[3]
千葉大学理学部
笠原順三・是沢定之・片尾浩[4]
東京大学地震研究所
海宝由佳[5]・金澤敏彦
東京大学理学部
塩原肇
北海道大学理学部
柏原静雄
気象庁
日野亮太
東北大学理学部
馬場久紀
東海大学海洋学部
久保篤規
神戸大学自然科学研究科

1) 現在　古川商業高等学校
2) 現在　東京大学海洋研究所
3) 現在　東京大学地震研究所
4) 現在　京都大学理学部
5) 現在　海洋科学技術センター

1989年，房総沖海溝三重会合点付近において，上部地殻を精密に求めるため，エアガン－海底地震計（OBS）を用いた地震波探査が行われた．22台のOBSを設置して，更に，気象庁の常時観測システムのOBS 4台とあわせて，計26台でアレイ観測を行った．このうち3台は，7000 mを超える深海に設置された．長さ300 km，巾80 kmの調査海域に，3本のエアガンの測線（全長450 km）を設けた．東西に引かれた測線では，水深が数100 mから9000 mまで変化している．同時に，房総半島においても臨時観測点を5箇所設けた．

震源は，2台の16リットルエアガンからなるアレイを用いた．発震間隔は40–50秒（約100 m）である．エアガンの信号は，OBSから30–40 km以上まで観測された．

堆積層を含む浅部地殻構造を求めるため，距離－時間軸断面の波形データと，それを原点走時－レイパラメーターの領域（τ－p領域）に変換した記録を解析した．τ–pの軌跡を読み取り，τ–sum inversion法によって速度構造を求めた．20台のOBS直下の堆積層の厚さとP波速度は大きく変化することが分かった．特に，海溝軸より陸側と海側では，はっきりした違いが認められた．海側の堆積層は，上部に音響的に透明な層（P波速度1.6 km/s，厚さ500 m，速度勾配，0.32 s^{-1}）と，不透明な層（約3 km/s，500 m，4.8 s^{-1}）がある．一方，東北日本側では，最上部透明層で速度勾配が0.65 s^{-1}，下部の不透明層で，0.8 s^{-1}と，速さが漸増し，全体の厚さは4 km以上ある．